

Quantum manipulation of asymmetric Einstein-Podolsky-Rosen steering in controllable dynamical Casimir arrays

Ruinian Li(李瑞年), Yumei Long(龙玉梅), and Xue Zhang(张雪)

Citation: Chin. Phys. B, 2025, 34 (**2**): 020307. DOI: 10.1088/1674-1056/ad9a99
Journal homepage: http://cpb.iphy.ac.cn; http://iopscience.iop.org/cpb

What follows is a list of articles you may be interested in

Enhancing entanglement and steering in a hybrid atom-optomechanical system via Duffing nonlinearity

Ling-Hui Dong(董凌晖), Xiao-Jie Wu(武晓捷), Cheng-Hua Bai(白成华), and Shao-Xiong Wu(武少雄)
Chin. Phys. B, 2025, 34 (**2**): 020304. DOI: 10.1088/1674-1056/ad9ba2

Generalized Einstein-Podolsky-Rosen steering paradox

Zhi-Jie Liu(刘志洁), Xing-Yan Fan(樊星言), Jie Zhou(周洁), Mi Xie(谢汨), and Jing-Ling Chen(陈景灵)
Chin. Phys. B, 2024, 33 (**11**): 110307. DOI: 10.1088/1674-1056/ad73b7

Ascertaining the influences of auxiliary qubits on the Einstein-Podolsky-Rosen steering and its directions

Ling-Ling Xing(邢玲玲), Huan Yang(杨欢), Gang Zhang(张刚), and Min Kong(孔敏)
Chin. Phys. B, 2024, 33 (**5**): 050304. DOI: 10.1088/1674-1056/ad1927

Genuine Einstein-Podolsky-Rosen steering of generalized three-qubit states via unsharp measurements

Yuyu Chen(陈玉玉), Fenzhuo Guo(郭奋卓), Shihui Wei(魏士慧), and Qiaoyan Wen(温巧燕)
Chin. Phys. B, 2023, 32 (**4**): 040309. DOI: 10.1088/1674-1056/acac14

Dynamical Casimir effect in superradiant light scattering by Bose–Einstein condensate in an optomechanical cavity

Sonam Mahajan, Neha Aggarwal, Aranya B Bhattacherjee, ManMohan
Chin. Phys. B, 2014, 23 (**2**): 020315. DOI: 10.1088/1674-1056/23/2/020315

Quantum manipulation of asymmetric Einstein–Podolsky–Rosen steering in controllable dynamical Casimir arrays

Ruinian Li(李瑞年), Yumei Long(龙玉梅)[†], and Xue Zhang(张雪)[‡]

Center for Quantum Sciences and School of Physics, Northeast Normal University, Changchun 130024, *China*

(Received 14 September 2024; revised manuscript received 18 November 2024; accepted manuscript online 5 December 2024)

We design dynamical Casimir arrays (DCA) consisting of giant atoms and coupled resonator waveguides (CRWs) to investigate the Einstein–Podolsky–Rosen (EPR) steering at finite temperatures. Our designed system exhibits an asymmetry in its structure, which is caused by the differences in the sizes and the coupling positions of the giant atoms. The system achieves different types of EPR steering and the reversal of one-way EPR steering by modulating parameters. Furthermore, the symmetry and asymmetry of the system structure, in their responses to parameter modulation, both reveal the asymmetry of EPR steering. In this process, we discover that with the increase in temperature, different types of steering can be transferred from Casimir photons to giant atoms. We also achieve the monogamy of the multipartite system. These results provide important assistance for secure quantum communication, and further intuitively validating the asymmetry of EPR steering from multiple perspectives.

Keywords: dynamical Casimir effect, EPR steering, monogamy relation, giant atoms, coupled resonator waveguides

PACS: 03.67.Hk, 03.67.Dd, 03.67.Mn

DOI: 10.1088/1674-1056/ad9a99 **CSTR:** 32038.14.CPB.ad9a99

1. Introduction

The dynamical Casimir effect (DCE) is a phenomenon that can produce pairs of photons from quantum vacuum fluctuations by means of the modulation of the mode structure of the quantum field.[1–6] Physicists designed a superconducting circuit terminated by a superconducting quantum interference device (SQUID) and observed the DCE.[7,8] These experiments not only observed the generation of real photon pairs, but also detected the quantum character of two-mode squeezing[9–11] in the production of photon pairs. Based on the unique quantum property of DCE, DCE is usually used as an appropriate quantum resource to discuss quantum correlation problems, such as quantum entanglement,[12–16] quantum discord[17–19] and Einstein–Podolsky–Rosen (EPR) steering.[20–28]

"EPR steering" was initially introduced by Schrödinger[29] in respond to the "spooky action at a distance" phenomenon indicated in the famous Einstein–Podolsky–Rosen (EPR) paradox[30] in 1935. It describes the ability of one party to nonlocally control the other party's states through local measurements, which reveals the inconsistency between local realism and the completeness of quantum mechanics.[21,30] From the perspective of quantum information,[20] EPR steering is a distinctive quantum correlation between quantum entanglement[12–16] and Bell nonlocality,[31] it corresponds to the task of validable entanglement distribution by an untrusted party. Due to the asymmetric quantum property of EPR steering, it plays a key role in one-sided device-independent quantum key distribution,[32–34] quantum teleportation,[35–37] subchannel discrimination,[38] and other related protocols. Driven by the future demand for quantum communication[39] security, as a key resource for building quantum network, EPR steering has expanded from bipartite to multipartite. For multipartite EPR steering,[40–43] it is composed of multiple spatially separated parties who cannot fully trust each other. With the investigation of how quantum resources are quantified and distributed, multipartite EPR steering has been deeply explored.

Here, we can choose the coupled resonator waveguides (CRWs) and the giant atoms to structure the quantum network. The CRW is an important physical model that can be realized by superconductor transmission line resonators.[44–47] Different from the continuum medium waveguides, CRW can provide special structures to manipulate the transport of photons,[44,46] so it can be used for quantum information processing.[23,32,38] Unlike conventional small atoms, the size of giant atoms is comparable to the wavelength of the propagation modes in the waveguide, so the dipole approximation is no longer valid. Since the first experimental study in 2014,[48] the structure of giant atoms can be realized in several systems such as superconducting qubits coupled to surface acoustic waves (SWAs)[49–52] or microwave transmission lines,[53–55] cold atoms interacting with dynamically dependent optical lattices.[56] Recently, the waveguide quantum

[†]Corresponding author. E-mail: longym158@nenu.edu.cn

[‡]Corresponding author. E-mail: zhangx800@nenu.edu.cn

© 2025 Chinese Physical Society and IOP Publishing Ltd. All rights, including for text and data mining, AI training, and similar technologies, are reserved.

electrodynamics based on giant atom has been extensively investigated.[54,57–59] A giant atom is nonlocally coupled to a waveguide via two coupling points, and the photon transport between these coupling points significantly alters the interaction between the giant atom and the waveguide. The emergence of giant atoms exhibits striking phenomena that have not been observed in traditional system, such as frequency-dependent relaxation,[49] non-exponential decay,[51,52,60] and decoherence-free interaction.[61–63]

On the basis of the superconducting quantum circuit which generates the DCE, we design more complex dynamical Casimir arrays (DCA) (see Fig. 1). In this paper, we have achieved the reversal and the monogamy relations[41,42] of EPR steering. In addition, we also discover some interesting phenomena, which we elaborate on in the main text. The structure of this paper is as follows. In Section 2, we present the model and Hamiltonian of the system. In Section 3, we introduce the theoretical basis and criteria for EPR steering. We show the results and discussion in Section 4. Subsection 4.1 discusses the inversion of EPR steering between giant atoms, Subsection 4.2 discusses the EPR steering from Casimir photons to giant atoms, Subsection 4.3 discusses monogamy relations in the EPR steering. We summarize this paper in Section 5.

2. Model and Hamiltonian

As sketched in Fig. 1(a), the system consists of two subsystems. Each subsystem is composed of a giant atom and a coupled resonator waveguide (CRW) consisting of N_c resonators, where each the giant atom couples to the waveguide via two positions. The giant atom serves as the two-level system. The two CRWs are connected and grounded through a superconducting quantum interference device (SQUID),[7] which acts as a moving mirror for the quantum superconducting system. By adjusting the external magnetic flux $\Phi_{\rm ext}$ of SQUID, it can generate the time-dependent boundary conditions. The waveguide-atom coupled system considered can be realized in superconducting quantum circuits, as demonstrated in Fig. 1(b). Here the LC circuits serve as the resonators. The Hamiltonian of the system is written as $H = H_{\rm C} + H_{\rm A} + H_{\rm I}$, where

$$\begin{aligned} H_{\rm C} =& \hbar\sum_{j}^{N_c}\omega_c^{(1)}a_j^\dagger a_j - \hbar\sum_{j}^{N_c}\xi^{(1)}\left(a_j^\dagger a_{j+1}+a_{j+1}^\dagger a_j\right) \\ &+\hbar\sum_{l}^{N_c}\omega_c^{(2)}a_l^\dagger a_l - \hbar\sum_{l}^{N_c}\xi^{(2)}\left(a_l^\dagger a_{l+1}+a_{l+1}^\dagger a_l\right), \quad (1) \end{aligned}$$

$$H_{\rm A} = \hbar\sum_{i=1}^{2}\Omega_i\frac{\sigma_z^i}{2}, \quad (2)$$

$$\begin{aligned} H_{\rm I} =& \hbar g_1\left[\left(a_{n_1}^\dagger + a_{n_2}^\dagger\right)\sigma_1^- + {\rm H.c.}\right] \\ &+\hbar g_2\left[\left(a_{m_1}^\dagger + a_{m_2}^\dagger\right)\sigma_2^- + {\rm H.c.}\right] \\ &+\hbar g_{k,f}(t)\left(a_{T_1}^\dagger + a_{T_1}\right)\left(a_{T_2}^\dagger + a_{T_2}\right). \quad (3) \end{aligned}$$

Here $\omega_c^{(1,2)}$ is the frequency of resonators in the 1st (2nd) waveguide. $a_{j(l)}^\dagger$, $a_{j(l)}$ are the creation and annihilation operators of the bosonic modes representing the $j(l)$-th resonator in the 1st (2nd) waveguide, respectively. $\xi^{(1,2)}$ is the coupling strength between the nearest resonators in the 1st (2nd) waveguide. N_c represents the total number of resonators in the waveguide. σ_z^i is the Pauli operator for the giant atoms, and Ω_i is the transition frequency of the giant atoms between the ground state and the excited state. $\sigma_i^\pm$ are the raising and lowering operators of the giant atoms. Two giant atoms are coupled to two waveguides via the n_1-th, n_2-th, m_1-th, and m_2-th sites with coupling strengths g_1 and g_2, respectively. The $g_{k,f}(t)$ represents the coupling strength between the two waveguides.

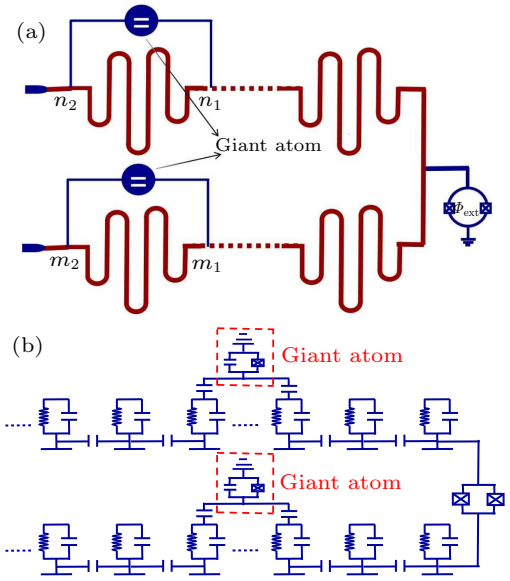


Fig. 1. (a) Diagram of the system, consisting of two subsystems composed of coupled resonator waveguides (CRWs) and giant atoms, where two giant atoms are coupled to the two waveguides via the n_1-th, n_2-th and m_1-th, m_2-th sites, respectively. (b) A equivalent circuit diagram of the system. The CRWs and giant atoms are represented by LC circuits and Transmons, respectively.

Furthermore, our system only considers single-mode forms, so the total creation operators for the two waveguides can be represented as $a_{T_1}^\dagger = a_k^\dagger$, $a_{T_2}^\dagger = a_f^\dagger$, respectively. Introducing the Fourier transformation

$$a_j = \frac{1}{\sqrt{N_c}}\sum_k a_k {\rm e}^{{\rm i}kj}, \quad a_l = \frac{1}{\sqrt{N_c}}\sum_f a_f {\rm e}^{{\rm i}fl}. \quad (4)$$

The Hamiltonian of the above system is described as

$$\begin{aligned} H =& \hbar\sum_{k=1}^{N_c}\omega_k a_k^\dagger a_k + \hbar\sum_{f=1}^{N_c}\omega_f a_f^\dagger a_f + \hbar\sum_{i=1}^{2}\Omega_i\frac{\sigma_z^i}{2} \\ &+\frac{\hbar g_1}{\sqrt{N_c}}\sum_k\left[\left({\rm e}^{-{\rm i}kn_1}+{\rm e}^{-{\rm i}kn_2}\right)a_k^\dagger\sigma_1^- + {\rm H.c.}\right] \\ &+\frac{\hbar g_2}{\sqrt{N_c}}\sum_f\left[\left({\rm e}^{-{\rm i}fm_1}+{\rm e}^{-{\rm i}fm_2}\right)a_f^\dagger\sigma_2^- + {\rm H.c.}\right] \\ &+\hbar g_{k,f}(t)\left(a_k^\dagger + a_k\right)\left(a_f^\dagger + a_f\right), \quad (5) \end{aligned}$$

where $\omega_{k,f} = \omega_{\rm c}^{(1,2)} - 2\xi^{(1,2)}\cos(k,f)$ represents the mode frequency of the waveguide. In what follows we provide a detailed introduction to the interaction term in the last line of Eq. (5). By changing the external magnetic flux $\phi_{\rm ext}$ of SQUID generates the time-dependent boundary conditions. It should be noted that the driving frequency $\omega_{\rm d}$ of SQUID must be less than its plasma frequency $\omega_{\rm p}$, therefore, the external flux $\phi_{\rm ext}(t)$ of SQUID is written as[13]

$$\frac{\phi_{\rm ext}}{2\varphi_0} = \bar{\phi} + \sum_{\langle k,f\rangle} \Delta_{k,f}\cos\left(\omega_{\rm d}^{k,f}t\right) \tag{6}$$

with $\omega_{\rm d} = \omega_k + \omega_f$, $\bar{\phi}$ is a constant offset and $\Delta_{k,f}$ is little variation, $\varphi_0 = \phi_0/2\pi$, ϕ_0 is magnetic flux quantum. The time-dependent coupling parameter $g_{k,l}(t)$ is given by[13]

$$g_{k,f}(t) = g_0^{k,f}\cos(\omega_{\rm d}t), \tag{7}$$

where

$$g_0^{k,f} = \frac{\varphi_0^2}{4E_J}\frac{\sin\bar{\phi}}{\cos^2\bar{\phi}}\sqrt{\frac{\omega_k\omega_f}{C_kC_f}}\frac{1}{Z_kZ_f}\Delta_{k,f}, \tag{8}$$

and $C_{k(f)}$ and $Z_{k(f)}$ are the corresponding capacitance and impedance of CRW$_{k(f)}$. According to Eqs. (6) and (8), controllable $\phi_{\rm ext}$ allows us to obtain tunable driving frequency and coupling strength $g_0^{k,f}$. Turning off the external flux of SQUID at reasonable time, the external driving and interaction of the waveguides will disappear.

3. Theoretical basis and criteria

3.1. Perturbative calculation

We employ the rotating wave approximation (RWA)[13,64] on the Hamiltonian of the waveguide–atom coupled system. Considering the giant atom is resonant with the waveguide, that is, $\omega_{k,f} = \Omega_i$. Therefore, in the interaction picture equation (5) is rewritten as

$$\begin{aligned} H_{\rm eff} =& \frac{\hbar g_1}{\sqrt{N_{\rm c}}}\sum_k\left[\left(\mathrm{e}^{-\mathrm{i}kn_1}+\mathrm{e}^{-\mathrm{i}kn_2}\right)a_k^\dagger\sigma_1^- + \text{H.c.}\right] \\ &+ \frac{\hbar g_2}{\sqrt{N_{\rm c}}}\sum_f\left[\left(\mathrm{e}^{-\mathrm{i}fm_1}+\mathrm{e}^{-\mathrm{i}fm_2}\right)a_f^\dagger\sigma_2^- + \text{H.c.}\right] \\ &+ \frac{\hbar g_0}{2}\left(a_k^\dagger a_f^\dagger + a_k a_f\right). \end{aligned} \tag{9}$$

In the experiments of superconducting quantum circuits, environmental temperature plays a crucial role. Therefore, we consider temperature in the system. The initial state of the waveguide–atom coupling system is

$$|\Phi(0)\rangle = \left|n_kn_f\right\rangle_{\rm CRW}\otimes|00\rangle_{\rm A}, \tag{10}$$

where

$$n_i = \left(\exp\left(\frac{\hbar\omega_i}{k_{\rm B}T_i}\right)-1\right)^{-1}, \quad (i=k,f), \tag{11}$$

is given by the Bose–Einstein distribution of the thermal photons. Here, $\hbar$, $k_{\rm B}$, T_i represent the reduced Planck constant, Boltzmann constant, and temperature of the system, respectively. We use the perturbative theory to derive the state $|\Phi(t)\rangle$ expanded up to the third order from state $|\Phi(0)\rangle$ under Eq. (9). The final state $|\Phi(t)\rangle$ can be written as linear superposition of the $|\Phi_n\rangle$, which are

$$\begin{aligned} &|a\rangle_{\rm CRW}\otimes|00\rangle_{\rm A}, \\ &a = n_kn_f,(n_k+1)(n_f+1),(n_k+2)(n_f+2), \\ &\quad (n_k+3)(n_f+3),(n_k-1)(n_f-1), \\ &\quad (n_k-2)(n_f-2),(n_k-3)(n_f-3), \\ &|b\rangle_{\rm CRW}\otimes|10\rangle_{\rm A}, \\ &b = (n_k-1)n_f,n_k(n_f+1),(n_k-2)(n_f-1), \\ &\quad (n_k+1)(n_f+2),(n_k-3)(n_f-2), \\ &|c\rangle_{\rm CRW}\otimes|01\rangle_{\rm A}, \\ &c = n_k(n_f-1),(n_k+1)n_f,(n_k-1)(n_f-2), \\ &\quad (n_k+2)(n_f+1),(n_k-2)(n_f-3), \\ &|d\rangle_{\rm CRW}\otimes|11\rangle_{\rm A}, \\ &d = n_kn_f,(n_k-1)(n_f-1),(n_k-2)(n_f-2), \\ &|e\rangle_{\rm CRW}\otimes|20\rangle_{\rm A}, \\ &e = (n_k-2)n_f,(n_k-1)(n_f+1),(n_k-3)(n_f-1), \\ &|g\rangle_{\rm CRW}\otimes|02\rangle_{\rm A}, \\ &g = n_k(n_f-2),(n_k+1)(n_f-1),(n_k-1)(n_f-3), \\ &|p\rangle_{\rm CRW}\otimes|21\rangle_{\rm A}, \\ &p = (n_k-2)(n_f-1), \\ &|x\rangle_{\rm CRW}\otimes|12\rangle_{\rm A}, \\ &x = (n_k-1)(n_f-2), \\ &|y\rangle_{\rm CRW}\otimes|30\rangle_{\rm A}, \\ &y = (n_k-3)n_f, \\ &|z\rangle_{\rm CRW}\otimes|03\rangle_{\rm A}, \\ &z = n_k(n_f-3). \end{aligned} \tag{12}$$

In terms of the average value formula $\langle A\rangle = \langle\Phi|A|\Phi\rangle$, we present average values expressed in the EPR criteria in the system. Some are shown here, and the rest of the values are shown in Appendix A:

$$\begin{aligned} &\langle\sigma_1\sigma_2\rangle \\ =& f^{(1,3)*}_{\left|(n_k-1)(n_f-1)\right\rangle_{\rm CRW}\otimes|00\rangle_{\rm A}} f^{(2)}_{\left|(n_k-1)(n_f-1)\right\rangle_{\rm CRW}\otimes|11\rangle_{\rm A}} \\ &+ f^{(2)*}_{\left|(n_k-2)(n_f-2)\right\rangle_{\rm CRW}\otimes|00\rangle_{\rm A}} f^{(3)}_{\left|(n_k-2)(n_f-2)\right\rangle_{\rm CRW}\otimes|11\rangle_{\rm A}} \\ &+ \sqrt{2} f^{(2)*}_{\left|(n_k-2)(n_f-1)\right\rangle_{\rm CRW}\otimes|10\rangle_{\rm A}} f^{(3)}_{\left|(n_k-2)(n_f-1)\right\rangle_{\rm CRW}\otimes|21\rangle_{\rm A}} \\ &+ \sqrt{2} f^{(2)*}_{\left|(n_k-1)(n_f-2)\right\rangle_{\rm CRW}\otimes|01\rangle_{\rm A}} f^{(3)}_{\left|(n_k-1)(n_f-2)\right\rangle_{\rm CRW}\otimes|12\rangle_{\rm A}} \\ &+ f^{(0,2)*}_{\left|n_kn_f\right\rangle_{\rm CRW}\otimes|00\rangle_{\rm A}} f^{(3)}_{\left|n_kn_f\right\rangle_{\rm CRW}\otimes|11\rangle_{\rm A}}, \\ &\langle\sigma_2\sigma_1\rangle \end{aligned}$$

$$
\begin{aligned}
= & f^{(1,3)*}_{\left|(n_k-1)(n_f-1)\right\rangle_{\mathrm{CRW}}\otimes|00\rangle_{\mathrm{A}}} f^{(2)}_{\left|(n_k-1)(n_f-1)\right\rangle_{\mathrm{CRW}}\otimes|11\rangle_{\mathrm{A}}} \\
& + f^{(2)*}_{\left|(n_k-2)(n_f-2)\right\rangle_{\mathrm{CRW}}\otimes|00\rangle_{\mathrm{A}}} f^{(3)}_{\left|(n_k-2)(n_f-2)\right\rangle_{\mathrm{CRW}}\otimes|11\rangle_{\mathrm{A}}} \\
& + \sqrt{2} f^{(2)*}_{\left|(n_k-2)(n_f-1)\right\rangle_{\mathrm{CRW}}\otimes|10\rangle_{\mathrm{A}}} f^{(3)}_{\left|(n_k-2)(n_f-1)\right\rangle_{\mathrm{CRW}}\otimes|21\rangle_{\mathrm{A}}} \\
& + \sqrt{2} f^{(2)*}_{\left|(n_k-1)(n_f-2)\right\rangle_{\mathrm{CRW}}\otimes|01\rangle_{\mathrm{A}}} f^{(3)}_{\left|(n_k-1)(n_f-2)\right\rangle_{\mathrm{CRW}}\otimes|12\rangle_{\mathrm{A}}} \\
& + f^{(0,2)*}_{\left|n_k n_f\right\rangle_{\mathrm{CRW}}\otimes|00\rangle_{\mathrm{A}}} f^{(3)}_{\left|n_k n_f\right\rangle_{\mathrm{CRW}}\otimes|11\rangle_{\mathrm{A}}}. \qquad (13)
\end{aligned}
$$

The coefficient f represents the transition amplitude of the system from the initial state to the corresponding state, and the superscripts indicate the orders in the perturbative expression at which the f appears. The transition amplitude formula is

$$
f_{nk}(t) = \frac{1}{\mathrm{i}\hbar}\int_{t_0}^{t} \langle n|\hat{H}|k\rangle \,\mathrm{d}t, \qquad (14)
$$

where $f_{nk}(t)$ represents the amplitude of the transition from an initial state $|k\rangle$ at time t_0 to a final state $|n\rangle$ at time t. Expressions of f are shown in Appendix A.

3.2. Criteria for the EPR steering

EPR steering criteria[65] proposed by Reid are typically used to study the EPR steering, and we employ the criteria to our system. Following the Refs. [65,66], the expression of the EPR steering criterion is

$$
w_{d_A\to d_B} = V_{\mathrm{inf}}\left(X_{d_B}\right) V_{\mathrm{inf}}\left(Y_{d_B}\right) < 1, \quad (d_A \to d_B), \qquad (15)
$$

or

$$
w_{d_B\to d_A} = V_{\mathrm{inf}}\left(X_{d_A}\right) V_{\mathrm{inf}}\left(Y_{d_A}\right) < 1, \quad (d_B \to d_A). \qquad (16)
$$

Here $X_{d_{A(B)}} = d_{A(B)} + d^{\dagger}_{A(B)}$ and $Y_{d_{A(B)}} = -\mathrm{i}\left(d_{A(B)} - d^{\dagger}_{A(B)}\right)$ are the quadrature operators. The variance involved in the formula is

$$
V_{\mathrm{inf}}(X_{d_B(d_A)}) = V(X_{d_B(d_A)}) - \frac{V^2(X_{d_B}, X_{d_A})}{V(X_{d_A(d_B)})}, \qquad (17)
$$

where $V(x) = \langle x^2\rangle - \langle x\rangle^2$ and $V(x,y) = \langle xy\rangle - \langle x\rangle\langle y\rangle$. In our system, d_A represents a_A or σ_A, d_B represents a_B or σ_B, where A and B are both constants and unequal. By substituting Eq. (17) into the criterion condition, simplifying and transforming the result, we obtain a witness[65] to determine whether the EPR steering occurs (for $A \neq B$).

$$
w_{d_A\to d_B} = \frac{\left\langle d^{\dagger}_B d_B\right\rangle\left(\left\langle d^{\dagger}_A d_A\right\rangle + 1/2\right)}{|\langle d_B d_A\rangle|^2} < 1, \qquad (18)
$$

$$
w_{d_B\to d_A} = \frac{\left\langle d^{\dagger}_A d_A\right\rangle\left(\left\langle d^{\dagger}_B d_B\right\rangle + 1/2\right)}{|\langle d_A d_B\rangle|^2} < 1. \qquad (19)
$$

If the steering criterion $w_{d_A\to d_B} < 1$ (or $w_{d_B\to d_A} < 1$) holds, there will be one-way EPR steering for $d_A \to d_B$ (or $d_B \to d_A$). It is worth noting that the one-way EPR steering only occurs when one of the two inequalities holds. If they hold simultaneously, there will be two-way EPR steering for $d_A \leftrightarrow d_B$.

4. Results and discussion

4.1. Inversion of EPR steering between giant atoms

In this section, we provide a detailed discussion on the EPR steering between two giant atoms in the model. Figure 2 shows the steering criterions of $w_{\sigma_1\to\sigma_2}$ and $w_{\sigma_2\to\sigma_1}$ over time. Taking Fig. 2(a) as an example, we choose the positions of coupling points are $n_1 = 50, n_2 = 58, m_1 = 50, m_2 = 52$. We observe that as time evolves, the appearance of one-way EPR steering $\sigma_1 \to \sigma_2$ occurs earlier than the one-way EPR steering $\sigma_2 \to \sigma_1$. Furthermore, with the continuation of time, two-way EPR steering $\sigma_1 \leftrightarrow \sigma_2$ emerges.

Therefore, we can choose to turn off the external driving flux of the SQUID at the appropriate time to obtain the desired one-way EPR steering or two-way EPR steering. In addition, we find that the reversal EPR steering can be achieved by adjusting the positions of the coupling points, such as setting $n_1 = 50$, $n_2 = 52$, $m_1 = 50$, $m_2 = 58$ as shown in Fig. 2(d). Building upon this concept, we can reselect the positions of the coupling points in a symmetrical manner and maintain equal temperatures in both waveguides, the reversal of EPR steering can be achieved by adjusting the coupling strength between the giant atoms and the waveguides, as shown in Figs. 2(b) and 2(e). Similarly, for an equal coupling strength ($g_1 = g_2 = 1.5\pi$ MHz), we adjust the positions of the coupling points while maintaining symmetry, we can achieve the reversal of EPR steering by manipulating the temperature of the waveguides, as shown in Figs. 2(c) and 2(f). Therefore, this approach allows us to control individual parameter, such as coupling position, coupling strength, or temperature, while keeping the other parameters fixed, the method to precisely control these parameters can enable the realization of EPR steering reversal between giant atoms.

Furthermore, since our waveguide is formed by a finite array of coupled resonators, where N_{c} is the number of resonators. We hypothesize that the length N_{c} of the waveguide chain plays a significant role in the steering between asymmetric giant atoms. In Fig. 3, we plot the steering $w_{\sigma_1\to\sigma_2}$ ($w_{\sigma_2\to\sigma_1}$) as a function of different waveguide chain lengths N_{c}. It is found that one-way EPR steering $\sigma_1 \to \sigma_2$ is achieved when N_{c} is set to 400, and one-way EPR steering $\sigma_2 \to \sigma_1$ is achieved when N_{c} is set to 600. Here, we can achieve the reversal of the one-way EPR steering by changing the N_{c}. Moreover, two-way EPR steering $\sigma_1 \leftrightarrow \sigma_2$ can be achieved when N_{c} is set to 100, 300, 700, 800, and 900. This result reveals that the one-way or two-way EPR steering relationship between giant atoms can also be achieved by adjusting the length of the waveguide chain. Unfortunately, during the construction of the system, in order to ensure the effectiveness of the approximation, we only investigated the scenario where the waveguide chain lengths of the two subsystems are equal. This limitation hinders our study of the complexity of superconducting quantum networks.

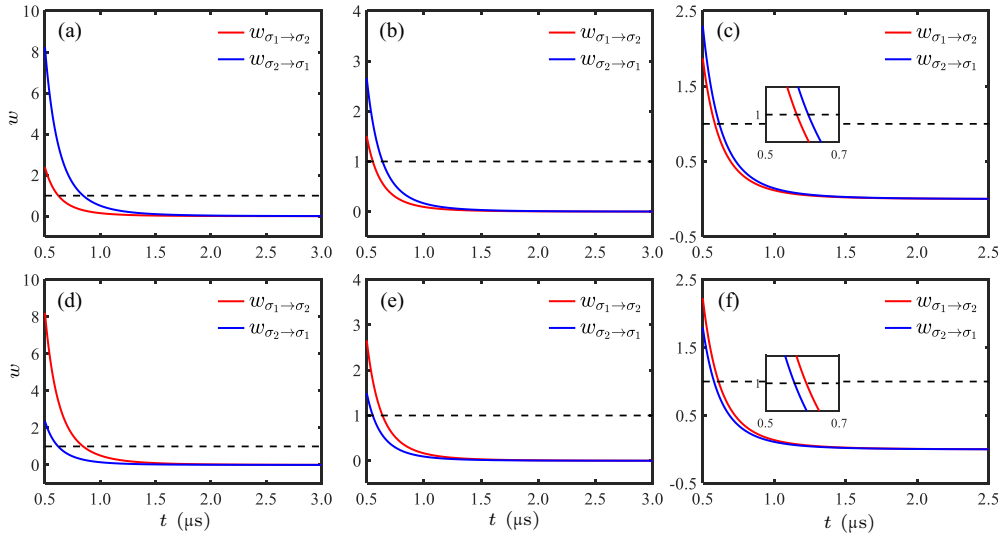


Fig. 2. The $w_{\sigma_1\to\sigma_2}$ and $w_{\sigma_2\to\sigma_1}$ as functions of time t. Here we use σ_1 and σ_2 represent two giant atoms. In panels (a) and (d), the coupling point positions we selected are $n_1 = 50$, $n_2 = 58$, $m_1 = 50$, $m_2 = 52$ in panel (a), $n_1 = 50$, $n_2 = 52$, $m_1 = 50$, $m_2 = 58$ in panel (d), the other parameters are $g_1 = g_2 = 1.5\pi$ MHz, $T_k = T_f = 60$ mK. In panels (b) and (e), the coupling strength between the giant atoms and the waveguides we selected are $g_1 = 2.0\pi$ MHz, $g_2 = 1.5\pi$ MHz in panel (b), $g_1 = 1.5\pi$ MHz, $g_2 = 2.0\pi$ MHz in panel (e), the other parameters are $n_1 = 52$, $n_2 = 58$, $m_1 = 52$, $m_2 = 58$, $T_k = T_f = 60$ mK. In panels (c) and (f), we choose the two waveguides temperatures with $T_k = 120$ mK, $T_f = 20$ mK in panel (c), $T_k = 20$ mK, $T_f = 120$ mK in panel (f), other parameters are $n_1 = 52$, $n_2 = 58$, $m_1 = 52$, $m_2 = 58$, $g_1 = g_2 = 1.5\pi$ MHz. Furthermore, we fix the number of resonators is $N_c = 200$, the coupling strength between the waveguides is $g_0 = 30\pi$ MHz, and the frequencies of the two waveguides are $\omega_k/2\pi = \omega_f/2\pi = 5$ GHz. The black dashed line in the figure represents a line with $w = 1$.

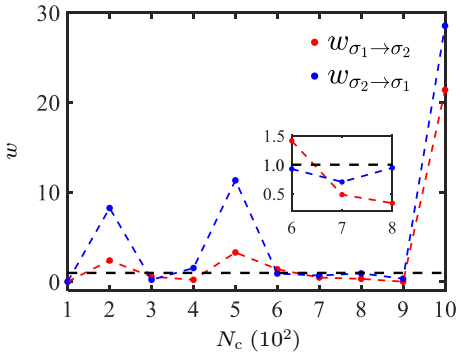


Fig. 3. The $w_{\sigma_1\to\sigma_2}$ (red scatter) and $w_{\sigma_2\to\sigma_1}$ (blue scatter) as functions of the waveguide chain length N_c. Here, we choose a fixed time $t = 0.5$ μs. Other parameters are the same as Fig. 2(a). The illustration represents the enlarged region of the horizontal coordinate spanning from 600 to 800.

In the preceding discussion, we mentioned that EPR steering between giant atoms can be reversed by exchanging the coupling coefficients. Therefore, in this paper, we detail the impact of the coupling strength between giant atoms and waveguides on the steering between giant atoms. Taking Fig. 4(a) as an example, we observe that the time for one-way EPR steering $\sigma_1 \to \sigma_2$ appears eariler than one-way EPR steering $\sigma_2 \to \sigma_1$ when $\mathcal{G} > 1$ and later than one-way EPR steering $\sigma_2 \to \sigma_1$ when $\mathcal{G} < 1$. Moreover, as $\mathcal{G}$ increases, the time of occurrence of one-way EPR steering $\sigma_1 \to \sigma_2$ becomes progressively earlier. For Fig. 4(b), the results of one-way EPR steering $\sigma_2 \to \sigma_1$ are found to be contrary to that. Therefore, when the coupling points of the giant atoms and the waveguides are symmetric, the giant atoms with a stronger coupling strength g_i $(i = 1, 2)$ leads the way in steering the giant atom with a weaker coupling strength g_i $(i = 1, 2)$. Moreover, as the coupling strength between the giant atoms and the waveguides increases, the time of occurrence of steering between the giant atoms becomes earlier. In addition, upon comparing Figs. 4(a) and 4(b), we find that the reversal of EPR steering can be accomplished by manipulating the ratio of coupling strengths $\mathcal{G}$. Hence, by manipulating the tunable coupling strengths, we can effectively control the desired types of steering as well as the generation and disappearance of steering. This feature offers valuable assistance in the preparation of multi-atom entangled states[67] and quantum information processing[23] in controllable superconducting quantum frameworks.

Remarkably, we observe that by comparing Figs. 4(a) and 4(c), all the plots of one-way EPR steering $\sigma_2 \to \sigma_1$ nearly coincide at the same position regardless of the choice of g_1. Moreover, by observing Fig. 4(f), we find that the plots coincide at the position where $\mathcal{G} = 1$ $(g_1 = g_2)$, indicating that the one-way EPR steering $\sigma_2 \to \sigma_1$ remains almost invariant with respect to variations in g_1. In other words, the one-way EPR steering $\sigma_2 \to \sigma_1$ exhibits robustness with respect to g_1, while the one-way EPR steering $\sigma_1 \to \sigma_2$ demonstrates a high sensitivity to variations in g_1. Upon comparing Figs. 4(b) and 4(d), with the opposite result. Therefore, by fixing a specific coupling strength, we can fix a corresponding one-way steering, while adjusting another coupling strength allows us to control the timing of the desired one-way steering. This sensitivity to the asymmetry of coupling strengths provides further compelling evidence for the asymmetry of EPR steering and offers a feasible approach for the implementation of quantum secure communication.

The preceding parts provide a detailed discussion about

the EPR steering between giant atoms. By adjusting the coupling position, coupling strength, temperature and the length of the waveguide chain, this system can not only enable the reversal of EPR steering between giant atoms, but also achieve the required one-way EPR steering and two-way EPR steering. In addition, we find a sensitive asymmetry of the steering with respect to the coupling strength. This method of effectively controlling parameters presents a suitable way to realize quantum information transmission[68] and secure quantum communication[35,39] in more complex quantum networks.

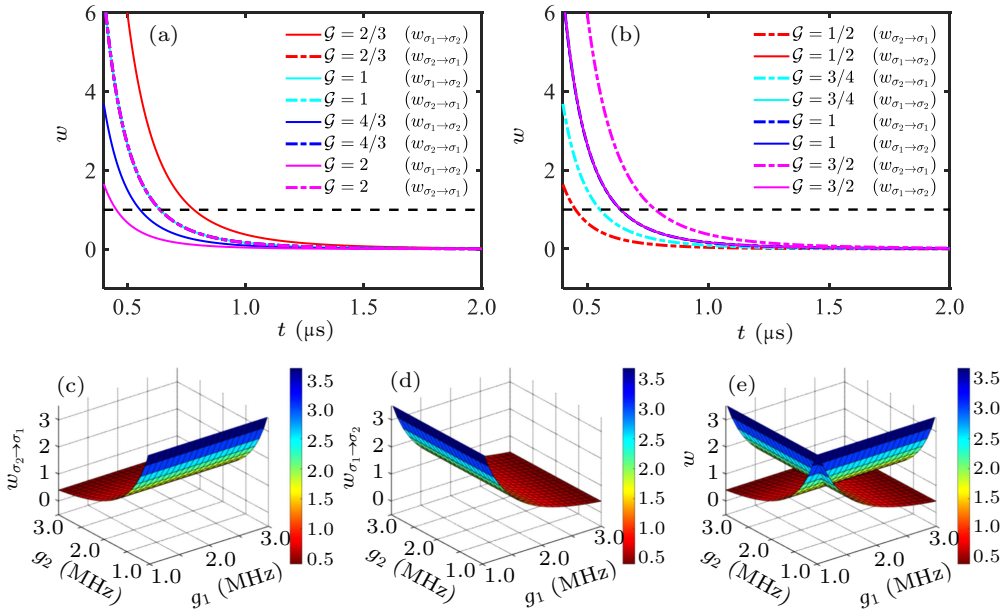


Fig. 4. Panels (a) and (b) respectively show the function graphs of $w_{\sigma_1\to\sigma_2}$ (solid lines) and $w_{\sigma_2\to\sigma_1}$ (dashed lines) over time in terms of different coupling strength ratio $\mathcal{G} = g_1/g_2$. We select the different values for $\mathcal{G}$ in panels (a) and (b). Panels (c) and (d) illustrate the three-dimensional (3D) surface plots of $w_{\sigma_1\to\sigma_2}$ and $w_{\sigma_2\to\sigma_1}$ as a function of the coupling strengths g_1 and g_2, respectively. Panel (f) represents the merged image of $w_{\sigma_1\to\sigma_2}$ and $w_{\sigma_2\to\sigma_1}$. Here, we choose a fixed time $t = 1$ μs. The other parameters are the same as Figs. 2(b) and 2(e).

4.2. EPR steering from Casimir photons to giant atoms

In previous sections, it was observed that temperature can serve as an effective controller for achieving steering reversal. Therefore, in this section, we investigate the influence of temperature on steering by treating it as a switch.

First, we attempt to utilize temperature as a switch to investigate its effects on the steering between giant atoms. As shown in Fig. 5(a), we maintain the temperature of two waveguides at the same value and deactivate the external magnetic flux at $t = 0.58$ μs. We observe that the image initially resembles a flat curve. However, as the temperature increases, around $T = 30$ mK, the image rapidly descends. Subsequently, one-way EPR steering $\sigma_1 \to \sigma_2$ and two-way EPR steering $\sigma_1 \leftrightarrow \sigma_2$ appear successively. Moreover, with further increase in temperature, two-way EPR steering persists throughout the process. Consequently, in Figs. 5(b) and 5(c), we observe one-way EPR steering $\sigma_1 \rightleftarrows \sigma_2$ by varying the temperature of both waveguides simultaneously. We find that as the temperature increases, the one-way EPR steering transitions from an initially non-steerable state to a steerable state, indicating that temperature can promote the revival of EPR steering between giant atoms. Interestingly, based on the asymmetry of the coupling point positions, we observe that the images of the steering with temperature are also asymmetric. Therefore, we present the reversed images of steering by swapping the positions of the coupling points in Fig. 5(a), as shown in Fig. 5(d), and provide the 3D plots of one-way EPR steering as a function of temperatures T_k and T_f, as shown in Figs. 5(e) and 5(f).

Taking Figs. 5(b) and 5(c) as examples, we observe that the one-way EPR steering $\sigma_1 \to \sigma_2$ exhibits sensitivity to the temperature T_k and T_f. The effect of temperature on one-way EPR steering is equivalent, displaying a certain degree of symmetry in its image. On the other hand, the one-way EPR steering $\sigma_2 \to \sigma_1$ shows sensitivity to temperature T_f and strong resistance to T_k, resulting in an asymmetric image. As for Figs. 5(e) and 5(f), the results are contrary to those. Regarding this phenomenon, we hypothesize that the temperature in the waveguides where giant atoms of different sizes are located is asymmetrically sensitive to the promotion of steering between giant atoms. Large-sized atoms take precedence in steering small-sized atoms, where the one-way EPR steering exhibits temperature sensitivity on the waveguide where the two different-sized giant atoms are located, such as $\sigma_1 \to \sigma_2$ in Fig. 5(b). When small-sized atoms steer large-sized atoms, the emergence of one-way EPR steering is temperature-sensitive for the small-sized atoms but resistant for the large-sized atoms, such as $\sigma_2 \to \sigma_1$ in Fig. 5(c). Therefore, we can control the appropriate temperatures (T_k and T_f) to select the desired type of steering. In the case of Figs. 5(b) and 5(c), by setting the temperature T_k of the waveguide to approach

absolute zero, selecting 150 mK $< T_f <$ 260 mK can lead to one-way EPR steering $\sigma_1 \to \sigma_2$, while choosing $T_f >$ 260 mK can lead to two-way EPR steering $\sigma_1 \leftrightarrow \sigma_2$. Similarly, taking Figs. 5(e) and 5(f) as examples, by setting the temperature T_k of the waveguide to approach absolute zero, selecting 100 mK $< T_f <$ 710 mK can lead to one-way EPR steering $\sigma_2 \to \sigma_1$, while choosing $T_f >$ 710 mK can lead to two-way EPR steering $\sigma_1 \leftrightarrow \sigma_2$. This instance demonstrates that the directionality is the unique property of EPR steering, which is different from both quantum entanglement and Bell nonlocality. It can be achieved by exchanging the positions of the coupling points to obtain one-way steering in opposite directions. This method of controlling EPR steering between giant atoms based on temperature can play a crucial role in the research of one-sided device-independent quantum key distribution[32] and subchannel discrimination.[38]

Next, we investigate the effect of temperature on the steering between Casimir photons. As shown in Fig. 6(a), we choose to close the external magnetic flux at $t = 0.0145$ μs, while maintaining $T_f = 60$ mK, to observe the variation of the steering image with T_f. The obtained steering plot initially demonstrates a flat curve and includes two-way EPR steering $a_k \leftrightarrow a_f$. In this temperature range, the steerings of $a_k \to a_f$ and $a_f \to a_k$ are robust to the temperature. However, with temperatures above 30 mK, one-way EPR steering $a_k \to a_f$ and $a_f \to a_k$ exponentially increased with temperature and rapidly vanished. Furthermore, by observing Figs. 6(b) and 6(c), it can be noted that temperature facilitates the sudden death of steering between photons, and the steering between photons is sensitive to temperature. Consequently, it is imperative to avoid excessively high temperatures in our system to prevent the disruption of EPR steering between photons.

In studying the temporal evolution of steering between photons, we observe a distinction from the investigation of giant atoms in that the available measurement means for manipulating steering between photons are limited. Under the premise of constructing two subsystems in complete symmetry, the controllability of steering is independent of the sizes of giant atoms, coupling positions, length of the waveguide chain, and the coupling strength between giant atoms and waveguides. It depends on the temperature, frequency of the waveguides, and the coupling strength between the waveguides.

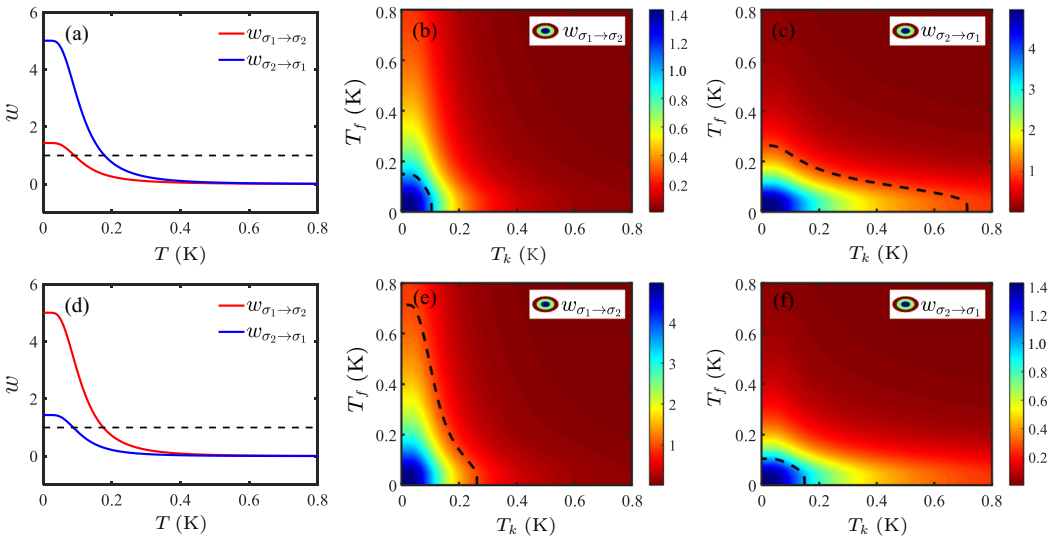


Fig. 5. Panels (a) and (d) illustrate the steering between two giant atoms as functions of temperature T. The temperatures of both waveguides are set to be the same, *i.e.*, $T_k = T_f = T$. Panels (b), (e) and (c), (f) respectively represent the variations of $w_{\sigma_1\to\sigma_2}$ and $w_{\sigma_2\to\sigma_1}$ with temperatures T_k and T_f. The time is fixed at $t = 0.58$ μs, the coupling point positions are chosen as $n_1 = 50$, $n_2 = 58$, $m_1 = 50$, $m_2 = 52$ in panels (a)–(c), and as $n_1 = 50$, $n_2 = 52$, $m_1 = 50$, $m_2 = 58$ in panels (d)–(f). Other parameters are $N_c = 200$, $g_0 = 30\pi$ MHz, $g_1 = g_2 = 1.5\pi$ MHz, $\omega_k/2\pi = \omega_f/2\pi = 5$ GHz. The black dashed line represents $w = 1$.

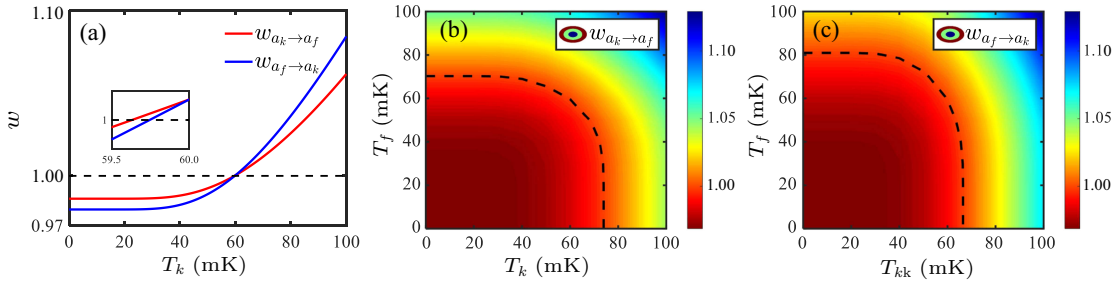


Fig. 6. Panel (a) illustrates the steering between two photons as functions of temperature T_k, one of the waveguides is held at a fixed temperature of $T_f = 60$ mK. Here we use a_k and a_f to represent the photons in the two waveguides. The variations of $w_{a_k\to a_f}$ and $w_{a_f\to a_k}$ with temperatures T_k and T_f in panels (b) and (c), respectively. The time is fixed at $t = 0.0145$ μs. The other parameters are the same as Fig. 2(c).

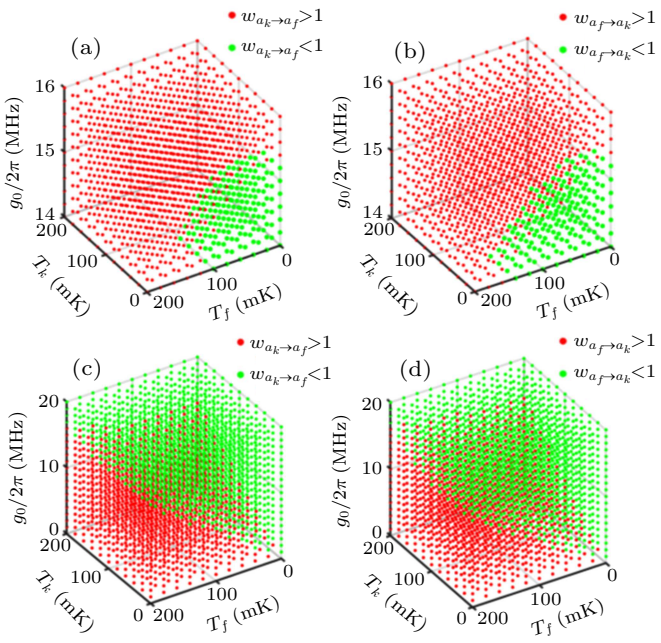


Fig. 7. Panels (a) and (b) display the 3D scatter plots of $w_{a_k\to a_f}$ and $w_{a_f\to a_k}$ as functions of the waveguide temperatures T_k and T_f and the coupling strength g_0 between the waveguids, where $\omega_k/2\pi = \omega_f/2\pi = 5$ GHz. Panels (c) and (d) display the 3D scatter plots of $w_{a_k\to a_f}$ and $w_{a_f\to a_k}$ as functions of the waveguide temperatures T_k and T_f and the waveguid frequency ω, where $g_0 = 30\pi$ MHz. The other parameters are the same as those in Fig. 6. In the plots, the red dots correspond to $w > 1$, while the green dots correspond to $w < 1$.

In order to establish a connection between them, we incorporate the coupling strength g_0 between waveguides into the measurement based on Figs. 6(b) and 6(c), and draw the steering as a 3D scatter plot with respect to temperature and coupling strength, as shown in Figs. 7(a) and 7(b). We find that as g_0 increase, the temperature range of feasible steerability between photons becomes smaller until it disappears. In other words, to ensure the existence of steering within the strong coupling regime, the system must be required to be at low temperatures. However, there still exists a critical threshold value that allows for steering between photons. If this critical threshold value is exceeded, the steering will not occur, regardless of how low the temperature is and how great the coupling strength is. This critical threshold value provides us with a valid reference range when preparing experimental devices to study steering, thereby preventing the destruction of steering. The two-way EPR steering in the presence of this critical threshold value ensures secure quantum teleportation[35–37] of photonic states. Additionally, we also draw the steering as a 3D scatter plot with respect to temperature and waveguide frequency, as shown in Figs. 7(c) and 7(d). We find that with the increase of the ω, the temperature range for steering between photons expands, eventually leading to complete occurrence. Hence, in the high-frequency regime, the system can effectively counteract the suppressive impact of temperature on the steering between photons, leading to the establishment of two-way EPR steering within the photons.

It is noteworthy that, given the assumption of symmetrical structures on the two subsystems, the one-way EPR steering $w_{a_k\to a_f}$ and $w_{a_f\to a_k}$ should theoretically exhibit identical images. However, the results are precisely the opposite. When g_0 is set to the same value in Figs. 7(a) and 7(b), or when ω is set to the same value in Figs. 7(c) and 7(d), we find that the steering images of $w_{a_k\to a_f}$ and $w_{a_f\to a_k}$ are not identical, this is also shown in Figs. 6(b) and 6(c). After analyzing inequalities (18) and (19), it becomes evident that when there are three variables, the functions related to them, such as n_k, n_f, and $f_{nk}(t)$, are operated in the form of 3D tensors, causing different matrices to emerge on each dimension, which in turn leads to distinct structures for $w_{a_k\to a_f}$ and $w_{a_f\to a_k}$. This intrinsic asymmetry is independent of the composition of the two subsystems, the asymmetry of EPR steering cannot be changed by parts of the whole system.

For the above process, we draw a steering evolution diagram as shown in Fig. 8. We make a comparison between the effects of temperature variation on the steering between giant atoms and the steering between Casimir photons. It was found that an increase in temperature significantly facilitated the sudden death of EPR steering between Casimir photons, suppressing their steerability, and thus leading to the disappearance of the EPR steering. However, it accelerated the occurrence of EPR steering between giant atoms, promoting the steering properties. In this process, the property of steering is transferred from Casimir photons to giant atoms. Therefore, selecting the appropriate temperature is crucial for guaranteeing the quantum information operation and transmission.

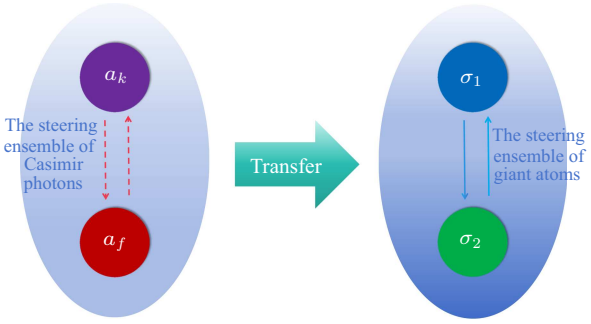


Fig. 8. The evolution diagram of EPR steering. The large ellipses represent the ensembles where steering exists, while the colored spheres denote Casimir photons and giant atoms. The small solid arrows represent the presence of steering and the small dashed arrows represent the disappearance of steering, whereas the large arrows signify the "transfer" of steering.

4.3. Monogamy relations in the EPR steering

Multipartite EPR steering is an important physical resource in quantum mechanics, which can be used in quantum communication and quantum computation. One of the most surprising features of multipartite EPR steering is that the monogamy, which quantifies the resources of quantum entanglement, cannot be shared freely between different constituents in a multipartite system. This feature ensures the

security of quantum cryptographic protocols and plays an important role in quantum information processing and device-independent protocols.[41,42,69] Here, we propose coupled CRWs and giant atoms in the DCA to investigate monogamy relations of multipartite EPR steering.

Due to the existence of the DCE, the virtual quantum fluctuations in the system are converted into real photons. Variations in photon number can affect the state of the surrounding field. Secondly, we note the interaction Hamiltonian between giant atoms and Casimir photons in Eq. (9), which can be used to swap states between photon modes and giant atom modes, thereby enabling quantum information swapping between different modes. First, we investigate the variation of monogamy relations with coupling strength g_0/ω_c and temperature T. We select the parameters within the dashed line range, e.g., when $1 \leq g_0/\omega_c\left(10^{-5}\right) \leq 6.2$, $0 < T \leq 37$ mK, a_f can steer σ_1 in Fig. 9(a), while σ_2 cannot steer σ_1 at the same region in Fig. 9(b). The phenomenon belongs to the type-I monogamy relation[42] of $a_f \to \sigma_1$, that is, two different modes cannot steer the same third mode simultaneously. However, if the parameter g_0/ω_c is tuned, the type-I monogamy relation of $a_f \to \sigma_1$ is lifted, and we can realize the type-I monogamy relation of $\sigma_2 \to \sigma_1$ in the case where $g_0/\omega_c\left(\times 10^{-4}\right) > 7.4$, as shown in Figs. 9(a) and 9(b). Therefore, in the three-mode combination a_f, σ_1, σ_2, as for a same steered party σ_1, the above process can be understood as the transition of steering party from a_f to σ_2, the system achieves the type-I monogamy relation swapping, as shown in Fig. 9(c). Similarly in the three-mode combination a_k, σ_1, σ_2, as for a same steered party σ_2, the system also realizes the type-I monogamy relation swapping for $(a_k \to \sigma_2) \Leftrightarrow (\sigma_1 \to \sigma_2)$($\Leftrightarrow$ repersents monogamy relation swapping) due to the conversion between steering party a_k and σ_1, as shown in Figs. 9(d)–9(f). Thus, our system can choose to obtain the desired monogamy relations in the appropriate temperature range and the coupling strength range.

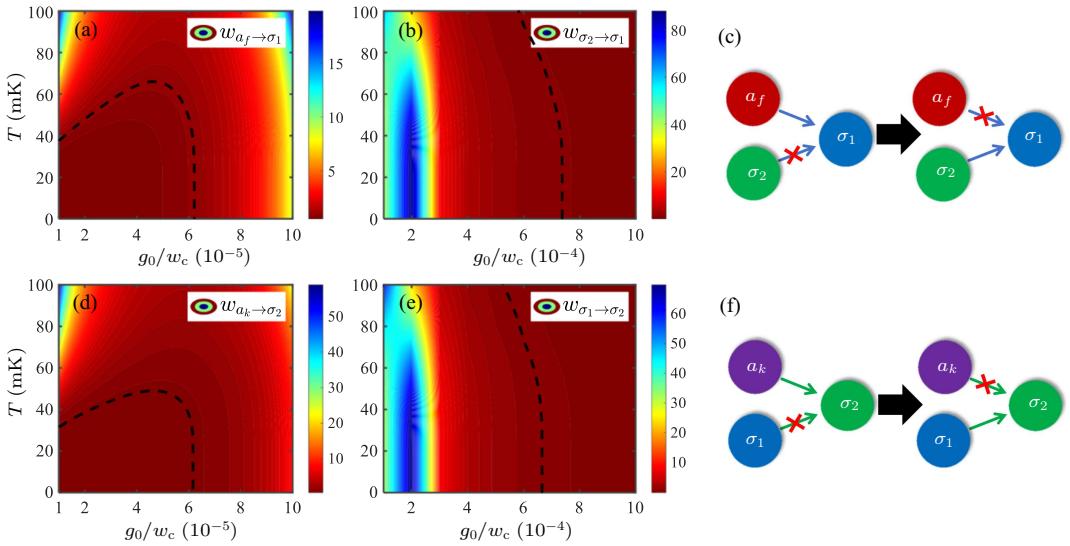


Fig. 9. The $w_{a_f\to\sigma_1}$, $w_{\sigma_2\to\sigma_1}$, $w_{a_k\to\sigma_2}$, and $w_{\sigma_1\to\sigma_2}$ as functions of coupling strength g_0/ω_c and temperature T ($T_k = T_f = T$) in panels (a), (b), (d), and (e), respectively. Panels (c) and (f) respectively correspond to the monogamy relations in each horizontal column, where the blue and green circles represent giant atoms, red and purple circles represent photons. The arrows indicate the presence of one-way EPR steering, while the red crosses represents no EPR steering. Other parameters are $n_1 = 50, n_2 = 52, m_1 = 70, m_2 = 72$, $N_c = 200$, $g_1 = g_2 = 1.5\pi$ MHz, $\omega_c/2\pi = 5$ GHz $t = 0.58$ μs. The black dashed line represents $w = 1$.

In addition, we also discuss the impact of changing the sizes of giant atoms and the couplings position of giant atoms on monogamy relations under three-mode combination. In Figs. 10(a) and 10(c), the nonlinear properties associated with the sizes of the giant atoms and the positions of the coupling points (n_1, n_2, m_1, m_2) lead to a more intricate impact on EPR steering. Therefore, we only consider the scenario where the sizes of the two giant atoms are identical, with fixed coupling positions at $n_1 = 50$ and $m_1 = 70$. The positions of the other two coupling points vary in the same trend S, $n_2 = 50 + S$, $m_2 = 70 + S$, where $S = 1, 2, \ldots, 9$. In Fig. 10(a), where σ_1 as the steered party, when $S = 1$, σ_2 can steer σ_1, but a_f cannot steer σ_1, which is the type-I monogamy relation of $\sigma_2 \to \sigma_1$. When $S = 2$, $\sigma_2 \to \sigma_1$ disappears and a_f can steer σ_1. With the increase of S, there is continuous swapping between steering parties, and the system realizes the type-I monogamy relation swapping for $(\sigma_2 \to \sigma_1) \Leftrightarrow (a_f \to \sigma_1)$. Likewise, for the same steered party σ_2, we also realize the conversion of the type-I monogamy relation $a_k \to \sigma_2$ and $\sigma_1 \to \sigma_2$ due to the conversion between steering party a_k and σ_1, as shown in Fig. 10(c).

Next, we maintain the same sizes of the two giant atoms to study the effect of the coupling positions of the giant atoms on the exchange of monogamy relations. Due to the bidirectional adjustability of the movements of the two giant atoms on the waveguides, we have a total of three mobility schemes, unidirectional fixed, bidirectional identical, and bidirectional

opposite. Here we only discuss the scenario of bidirectional opposition, where we move the positions of the first giant atom by "$-p$" and the positions of the second giant atom by "$+p$". In Fig. 10(b), we choose $p=-9$, σ_2 can steer σ_1, but a_f cannot simultaneously steer σ_1, which is the type-I monogamy relation $\sigma_2 \to \sigma_1$. When we choose $p=-7$, $\sigma_2 \to \sigma_1$ disappears and a_f can steer σ_1. With the increase of p, we find that the system realizes the type-I monogamy relation swapping for $(\sigma_2 \to \sigma_1) \Leftrightarrow (a_f \to \sigma_1)$. Similarly, for the same steered party σ_2, we realize the conversion of type-I monogamy relation between $a_k \to \sigma_2$ and $\sigma_1 \to \sigma_2$ by converting the steering party a_k and σ_1, as shown in Fig. 10(d). The above discussion confirms that the exchange of monogamy relations in the system can be achieved by adjusting the sizes of giant atoms and the coupling positions of giant atoms.

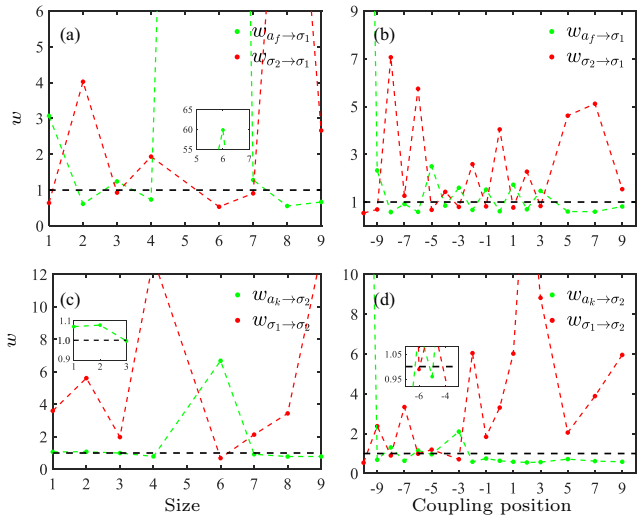


Fig. 10. The $w_{a_f\to\sigma_1}$, $w_{\sigma_2\to\sigma_1}$, $w_{a_k\to\sigma_2}$, and $w_{\sigma_1\to\sigma_2}$ as functions of the sizes of the giant atoms in panels (a) and (c), respectively. Select $n_1=50$, $m_1=70$, $n_2=50+S$, $m_2=70+S$, $(S=1,2,\ldots,9)$, $T_f=40$ mK. The $w_{a_f\to\sigma_1}$, $w_{\sigma_2\to\sigma_1}$, $w_{a_k\to\sigma_2}$, and $w_{\sigma_1\to\sigma_2}$ as functions of the coupling positions of the giant atoms in panels (b) and (d), respectively. We select $n_1=50-p$, $n_2=52-p$, $m_1=70+p$, $m_2=72+p$, $(p=-9,\ldots,9)$, $T_f=20$ mK. The other parameters are $N_c=200$, $g_1=g_2=1.5\pi$ MHz, $g_0=0.2\pi$ MHz, $\omega_k/2\pi=\omega_f/2\pi=5$ GHz, $T_k=20$ mK, $t=0.75$ μs.

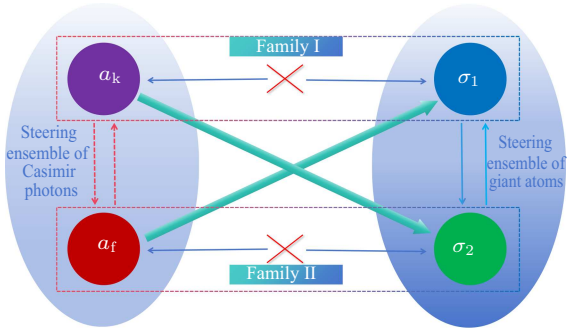


Fig. 11. The evolution diagram of EPR steering. The large ellipses represent the ensembles where steering exists, while the colored spheres denote Casimir photons and giant atoms. The dashed boxes indicate distinct "families" composed of giant atoms and Casimir photons generated within the same subsystem. Solid arrows represent the presence of steering, while dashed arrows indicate the disappearance of steering. Red crosses indicate the absence of steering.

We are dedicated to constructing more complex DCA, within which investigating EPR steering between giant atoms and Casimir photons constitutes a novel approach. We observe that with parameter adjustments, the steering between Casimir photons disappears, and then the steering between giant atoms emerges, as well as the steering from Casimir photons to giant atoms. Furthermore, we note that members belonging to the same "family" do not exhibit steering among themselves, as shown in Fig. 11. Taking the example of a_k and σ_1 in family I from Fig. 11, by transforming Inequality (18) into the form

$$w_{d_A\to d_B}=\left\langle d_B^\dagger d_B\right\rangle\left(\left\langle d_A^\dagger d_A\right\rangle+\frac{1}{2}\right)-|\langle d_B d_A\rangle|^2<0,$$

it can be inferred that a steering exists when $w_{d_A\to d_B}<0$. For $w_{a_k\to\sigma_1}$, since $\langle\sigma_1 a_k\rangle=0$, it follows that

$$w_{a_k\to\sigma_1}=\left\langle\sigma_1^\dagger\sigma_1\right\rangle\left(\left\langle a_k^\dagger a_k\right\rangle+\frac{1}{2}\right)>0.$$

Similarly, the same applies to $w_{\sigma_1\to a_k}$, meaning that no steering will arise between a_k and σ_1. These phenomena allow us to have a better understanding of the essence of steering. Furthermore, in such DCA, we can manipulate the conversion of steered parties by adjusting various parameters, thereby obtaining conversion of type-I monogamy relations. These results are useful for exploring the entanglement theory, quantum information processing and secure quantum communication.

5. Conclusion

We have discussed the EPR steering in the DCA consisting of giant atoms and coupled resonator waveguides. The specific results obtained through calculation and image analysis are as follows.

We utilized the external driving flux of the SQUID as a switch to control the "on-off" state of the circuit, thereby achieving the desired EPR steering for our research purposes. By adjusting the position of the coupling point, the coupling strength, the temperature, and the length of the waveguide chain, we not only achieved one-way or two-way EPR steering, but also realized the reversal of the one-way EPR steering between giant atoms. Furthermore, the differences in the characteristics of the giant atoms, specifically their sizes and coupling positions, primarily lead to the asymmetry of the system structure. The response of the asymmetry of the system structure to the changes in waveguide chain length and coupling strength reflects the asymmetry of EPR steering between giant atoms. Additionally, the asymmetry of the system structure in response to temperature results in different temperature ranges for EPR steering survival. Finally, we have discovered that with the increase in temperature, steering can be transferred from Casimir photons to giant atoms. We have achieved the converting of steering parties by selecting suitable ranges of coupling strength and temperature, or by selecting appropriate sizes and coupling positions of the giant atoms, thus realizing

the swapping of type-I monogamy relations. Here, the study of the sizes and coupling positions of giant atoms facilitates the regulation and control of multipartite EPR steering in our system.

Under the framework of superconducting quantum circuit, we provide an effective idea for researching EPR steering by constructing complex DCA and utilizing simple modulation means. We have also verified the asymmetry of EPR steering in multiple aspects, making significant contributions to the field of quantum key distribution and other areas. In summary, based on all the above conclusions, the paper contributes to the construction of more complex quantum networks, as well as for the research and development of quantum information and secure quantum communication.

Appendix A

We exhibit some average values $\langle d_A d_B\rangle$ and $\langle d_A^\dagger d_A\rangle$ in Section 3, the rest of the values are expressed as follows:

$$
\begin{aligned}
\left\langle a_k^\dagger a_k\right\rangle =\ & (n_k+1)\left|f^{(1,3)}_{|(n_k+1)(n_f+1)\rangle_{\mathrm{CRW}}\otimes|00\rangle_{\mathrm{A}}}\right|^2+(n_k+1)\left|f^{(2)}_{|(n_k+1)n_f\rangle_{\mathrm{CRW}}\otimes|01\rangle_{\mathrm{A}}}\right|^2+(n_k+1)\left|f^{(3)}_{|(n_k+1)(n_f+2)\rangle_{\mathrm{CRW}}\otimes|10\rangle_{\mathrm{A}}}\right|^2\\
&+(n_k+1)\left|f^{(3)}_{|(n_k+1)(n_f-1)\rangle_{\mathrm{CRW}}\otimes|02\rangle_{\mathrm{A}}}\right|^2+(n_k+2)\left|f^{(2)}_{|(n_k+2)(n_f+2)\rangle_{\mathrm{CRW}}\otimes|00\rangle_{\mathrm{A}}}\right|^2+(n_k+2)\left|f^{(3)}_{|(n_k+2)(n_f+1)\rangle_{\mathrm{CRW}}\otimes|01\rangle_{\mathrm{A}}}\right|^2\\
&+(n_k+3)\left|f^{(3)}_{|(n_k+3)(n_f+3)\rangle_{\mathrm{CRW}}\otimes|00\rangle_{\mathrm{A}}}\right|^2+(n_k-1)\left|f^{(1,3)}_{|(n_k-1)n_f\rangle_{\mathrm{CRW}}\otimes|10\rangle_{\mathrm{A}}}\right|^2+(n_k-1)\left|f^{(1,3)}_{|(n_k-1)(n_f-1)\rangle_{\mathrm{CRW}}\otimes|00\rangle_{\mathrm{A}}}\right|^2\\
&+(n_k-1)\left|f^{(2)}_{|(n_k-1)(n_f-1)\rangle_{\mathrm{CRW}}\otimes|11\rangle_{\mathrm{A}}}\right|^2+(n_k-1)\left|f^{(2)}_{|(n_k-1)(n_f-2)\rangle_{\mathrm{CRW}}\otimes|01\rangle_{\mathrm{A}}}\right|^2+(n_k-1)\left|f^{(3)}_{|(n_k-1)(n_f+1)\rangle_{\mathrm{CRW}}\otimes|20\rangle_{\mathrm{A}}}\right|^2\\
&+(n_k-1)\left|f^{(3)}_{|(n_k-1)(n_f-2)\rangle_{\mathrm{CRW}}\otimes|12\rangle_{\mathrm{A}}}\right|^2+(n_k-1)\left|f^{(3)}_{|(n_k-1)(n_f-3)\rangle_{\mathrm{CRW}}\otimes|02\rangle_{\mathrm{A}}}\right|^2+(n_k-2)\left|f^{(2)}_{|(n_k-2)n_f\rangle_{\mathrm{CRW}}\otimes|20\rangle_{\mathrm{A}}}\right|^2\\
&+(n_k-2)\left|f^{(2)}_{|(n_k-2)(n_f-1)\rangle_{\mathrm{CRW}}\otimes|10\rangle_{\mathrm{A}}}\right|^2+(n_k-2)\left|f^{(2)}_{|(n_k-2)(n_f-2)\rangle_{\mathrm{CRW}}\otimes|00\rangle_{\mathrm{A}}}\right|^2+(n_k-2)\left|f^{(3)}_{|(n_k-2)(n_f-1)\rangle_{\mathrm{CRW}}\otimes|21\rangle_{\mathrm{A}}}\right|^2\\
&+(n_k-2)\left|f^{(3)}_{|(n_k-2)(n_f-2)\rangle_{\mathrm{CRW}}\otimes|11\rangle_{\mathrm{A}}}\right|^2+(n_k-2)\left|f^{(3)}_{|(n_k-2)(n_f-3)\rangle_{\mathrm{CRW}}\otimes|01\rangle_{\mathrm{A}}}\right|^2+(n_k-3)\left|f^{(3)}_{|(n_k-3)n_f\rangle_{\mathrm{CRW}}\otimes|30\rangle_{\mathrm{A}}}\right|^2\\
&+(n_k-3)\left|f^{(3)}_{|(n_k-3)(n_f-1)\rangle_{\mathrm{CRW}}\otimes|20\rangle_{\mathrm{A}}}\right|^2+(n_k-3)\left|f^{(3)}_{|(n_k-3)(n_f-2)\rangle_{\mathrm{CRW}}\otimes|10\rangle_{\mathrm{A}}}\right|^2+(n_k-3)\left|f^{(3)}_{|(n_k-3)(n_f-3)\rangle_{\mathrm{CRW}}\otimes|00\rangle_{\mathrm{A}}}\right|^2\\
&+n_k\left|f^{(0,2)}_{|n_k n_f\rangle_{\mathrm{CRW}}\otimes|00\rangle_{\mathrm{A}}}\right|^2+n_k\left|f^{(1,3)}_{|n_k(n_f-1)\rangle_{\mathrm{CRW}}\otimes|01\rangle_{\mathrm{A}}}\right|^2+n_k\left|f^{(2)}_{|n_k(n_f+1)\rangle_{\mathrm{CRW}}\otimes|10\rangle_{\mathrm{A}}}\right|^2\\
&+n_k\left|f^{(2)}_{|n_k(n_f-2)\rangle_{\mathrm{CRW}}\otimes|02\rangle_{\mathrm{A}}}\right|^2+n_k\left|f^{(3)}_{|n_k n_f\rangle_{\mathrm{CRW}}\otimes|11\rangle_{\mathrm{A}}}\right|^2+n_k\left|f^{(3)}_{|n_k(n_f-3)\rangle_{\mathrm{CRW}}\otimes|03\rangle_{\mathrm{A}}}\right|^2,\\
\left\langle\sigma_1^\dagger\sigma_1\right\rangle =\ & \left|f^{(1,3)}_{|(n_k-1)n_f\rangle_{\mathrm{CRW}}\otimes|10\rangle_{\mathrm{A}}}\right|^2+\left|f^{(2)}_{|(n_k-1)(n_f-1)\rangle_{\mathrm{CRW}}\otimes|11\rangle_{\mathrm{A}}}\right|^2+\left|f^{(2)}_{|n_k(n_f+1)\rangle_{\mathrm{CRW}}\otimes|10\rangle_{\mathrm{A}}}\right|^2+\left|f^{(2)}_{|(n_k-2)(n_f-1)\rangle_{\mathrm{CRW}}\otimes|10\rangle_{\mathrm{A}}}\right|^2\\
&+\left|f^{(3)}_{|(n_k-1)(n_f-2)\rangle_{\mathrm{CRW}}\otimes|12\rangle_{\mathrm{A}}}\right|^2+\left|f^{(3)}_{|n_k n_f\rangle_{\mathrm{CRW}}\otimes|11\rangle_{\mathrm{A}}}\right|^2+\left|f^{(3)}_{|(n_k-2)(n_f-2)\rangle_{\mathrm{CRW}}\otimes|11\rangle_{\mathrm{A}}}\right|^2+\left|f^{(3)}_{|(n_k+1)(n_f+2)\rangle_{\mathrm{CRW}}\otimes|10\rangle_{\mathrm{A}}}\right|^2\\
&+\left|f^{(3)}_{|(n_k-3)(n_f-2)\rangle_{\mathrm{CRW}}\otimes|10\rangle_{\mathrm{A}}}\right|^2+2\left|f^{(2)}_{|(n_k-2)n_f\rangle_{\mathrm{CRW}}\otimes|20\rangle_{\mathrm{A}}}\right|^2+2\left|f^{(3)}_{|(n_k-2)(n_f-1)\rangle_{\mathrm{CRW}}\otimes|21\rangle_{\mathrm{A}}}\right|^2+2\left|f^{(3)}_{|(n_k-1)(n_f+1)\rangle_{\mathrm{CRW}}\otimes|20\rangle_{\mathrm{A}}}\right|^2\\
&+2\left|f^{(3)}_{|(n_k-3)(n_f-1)\rangle_{\mathrm{CRW}}\otimes|20\rangle_{\mathrm{A}}}\right|^2+3\left|f^{(3)}_{|(n_k-3)n_f\rangle_{\mathrm{CRW}}\otimes|30\rangle_{\mathrm{A}}}\right|^2,\\
\left\langle\sigma_2^\dagger\sigma_2\right\rangle =\ & \left|f^{(1,3)}_{|n_k(n_f-1)\rangle_{\mathrm{CRW}}\otimes|01\rangle_{\mathrm{A}}}\right|^2+\left|f^{(2)}_{|(n_k-1)(n_f-1)\rangle_{\mathrm{CRW}}\otimes|11\rangle_{\mathrm{A}}}\right|^2+\left|f^{(2)}_{|(n_k+1)n_f\rangle_{\mathrm{CRW}}\otimes|01\rangle_{\mathrm{A}}}\right|^2+\left|f^{(2)}_{|(n_k-1)(n_f-2)\rangle_{\mathrm{CRW}}\otimes|01\rangle_{\mathrm{A}}}\right|^2\\
&+\left|f^{(3)}_{|(n_k-2)(n_f-1)\rangle_{\mathrm{CRW}}\otimes|21\rangle_{\mathrm{A}}}\right|^2+\left|f^{(3)}_{|n_k n_f\rangle_{\mathrm{CRW}}\otimes|11\rangle_{\mathrm{A}}}\right|^2+\left|f^{(3)}_{|(n_k-2)(n_f-2)\rangle_{\mathrm{CRW}}\otimes|11\rangle_{\mathrm{A}}}\right|^2+\left|f^{(3)}_{|(n_k+2)(n_f+1)\rangle_{\mathrm{CRW}}\otimes|01\rangle_{\mathrm{A}}}\right|^2\\
&+\left|f^{(3)}_{|(n_k-2)(n_f-3)\rangle_{\mathrm{CRW}}\otimes|01\rangle_{\mathrm{A}}}\right|^2+2\left|f^{(2)}_{|n_k(n_f-2)\rangle_{\mathrm{CRW}}\otimes|02\rangle_{\mathrm{A}}}\right|^2+2\left|f^{(3)}_{|(n_k-1)(n_f-2)\rangle_{\mathrm{CRW}}\otimes|12\rangle_{\mathrm{A}}}\right|^2+2\left|f^{(3)}_{|(n_k+1)(n_f-1)\rangle_{\mathrm{CRW}}\otimes|02\rangle_{\mathrm{A}}}\right|^2\\
&+2\left|f^{(3)}_{|(n_k-1)(n_f-3)\rangle_{\mathrm{CRW}}\otimes|02\rangle_{\mathrm{A}}}\right|^2+3\left|f^{(3)}_{|n_k(n_f-3)\rangle_{\mathrm{CRW}}\otimes|03\rangle_{\mathrm{A}}}\right|^2,\\
\langle a_k a_f\rangle =\ & \langle a_f a_k\rangle\\
=\ & \sqrt{n_k n_f}f^{(1,3)*}_{|(n_k-1)(n_f-1)\rangle_{\mathrm{CRW}}\otimes|00\rangle_{\mathrm{A}}}f^{(0,2)}_{|n_k n_f\rangle_{\mathrm{CRW}}\otimes|00\rangle_{\mathrm{A}}}+\sqrt{n_k n_f}f^{(2)*}_{|(n_k-1)(n_f-1)\rangle_{\mathrm{CRW}}\otimes|11\rangle_{\mathrm{A}}}f^{(3)}_{|n_k n_f\rangle_{\mathrm{CRW}}\otimes|11\rangle_{\mathrm{A}}}\\
&+\sqrt{(n_k-1)n_f}f^{(2)*}_{|(n_k-2)(n_f-1)\rangle_{\mathrm{CRW}}\otimes|10\rangle_{\mathrm{A}}}f^{(1,3)}_{|(n_k-1)n_f\rangle_{\mathrm{CRW}}\otimes|10\rangle_{\mathrm{A}}}+\sqrt{n_k\left(n_f-1\right)}f^{(2)*}_{|(n_k-1)(n_f-2)\rangle_{\mathrm{CRW}}\otimes|01\rangle_{\mathrm{A}}}f^{(1,3)}_{|n_k(n_f-1)\rangle_{\mathrm{CRW}}\otimes|01\rangle_{\mathrm{A}}}\\
&+\sqrt{(n_k+1)\left(n_f+1\right)}f^{(0,2)*}_{|n_k n_f\rangle_{\mathrm{CRW}}\otimes|00\rangle_{\mathrm{A}}}f^{(1,3)}_{|(n_k+1)(n_f+1)\rangle_{\mathrm{CRW}}\otimes|00\rangle_{\mathrm{A}}}+\sqrt{(n_k-1)\left(n_f-1\right)}f^{(2)*}_{|(n_k-2)(n_f-2)\rangle_{\mathrm{CRW}}\otimes|00\rangle_{\mathrm{A}}}f^{(1,3)}_{|(n_k-1)(n_f-1)\rangle_{\mathrm{CRW}}\otimes|00\rangle_{\mathrm{A}}}\\
&+\sqrt{(n_k-2)n_f}f^{(3)*}_{|(n_k-3)(n_f-1)\rangle_{\mathrm{CRW}}\otimes|20\rangle_{\mathrm{A}}}f^{(2)}_{|(n_k-2)n_f\rangle_{\mathrm{CRW}}\otimes|20\rangle_{\mathrm{A}}}+\sqrt{(n_k-1)\left(n_f-1\right)}f^{(3)*}_{|(n_k-2)(n_f-2)\rangle_{\mathrm{CRW}}\otimes|11\rangle_{\mathrm{A}}}f^{(2)}_{|(n_k-1)(n_f-1)\rangle_{\mathrm{CRW}}\otimes|11\rangle_{\mathrm{A}}}\\
&+\sqrt{n_k\left(n_f+1\right)}f^{(1,3)*}_{|(n_k-1)n_f\rangle_{\mathrm{CRW}}\otimes|10\rangle_{\mathrm{A}}}f^{(2)}_{|n_k(n_f+1)\rangle_{\mathrm{CRW}}\otimes|10\rangle_{\mathrm{A}}}+\sqrt{(n_k-2)\left(n_f-1\right)}f^{(3)*}_{|(n_k-3)(n_f-2)\rangle_{\mathrm{CRW}}\otimes|10\rangle_{\mathrm{A}}}f^{(2)}_{|(n_k-2)(n_f-1)\rangle_{\mathrm{CRW}}\otimes|10\rangle_{\mathrm{A}}}\\
&+\sqrt{n_k\left(n_f-2\right)}f^{(3)*}_{|(n_k-1)(n_f-3)\rangle_{\mathrm{CRW}}\otimes|02\rangle_{\mathrm{A}}}f^{(2)}_{|n_k(n_f-2)\rangle_{\mathrm{CRW}}\otimes|02\rangle_{\mathrm{A}}}+\sqrt{(n_k+1)n_f}f^{(1,3)*}_{|n_k(n_f-1)\rangle_{\mathrm{CRW}}\otimes|01\rangle_{\mathrm{A}}}f^{(2)}_{|(n_k+1)n_f\rangle_{\mathrm{CRW}}\otimes|01\rangle_{\mathrm{A}}}\\
&+\sqrt{(n_k-1)\left(n_f-2\right)}f^{(3)*}_{|(n_k-2)(n_f-3)\rangle_{\mathrm{CRW}}\otimes|01\rangle_{\mathrm{A}}}f^{(2)}_{|(n_k-1)(n_f-2)\rangle_{\mathrm{CRW}}\otimes|01\rangle_{\mathrm{A}}}
\end{aligned}
$$

$$
\begin{aligned}
&+\sqrt{(n_k+2)(n_f+2)}f^{(1,3)*}_{|(n_k+1)(n_f+1)\rangle_{\mathrm{CRW}}\otimes|00\rangle_{\mathrm{A}}}f^{(2)}_{|(n_k+2)(n_f+2)\rangle_{\mathrm{CRW}}\otimes|00\rangle_{\mathrm{A}}}\\
&+\sqrt{(n_k-2)(n_f-2)}f^{(3)*}_{|(n_k-3)(n_f-3)\rangle_{\mathrm{CRW}}\otimes|00\rangle_{\mathrm{A}}}f^{(2)}_{|(n_k-2)(n_f-2)\rangle_{\mathrm{CRW}}\otimes|00\rangle_{\mathrm{A}}}\\
&+\sqrt{(n_k-1)(n_f+1)}f^{(2)*}_{|(n_k-2)n_f\rangle_{\mathrm{CRW}}\otimes|20\rangle_{\mathrm{A}}}f^{(3)}_{|(n_k-1)(n_f+1)\rangle_{\mathrm{CRW}}\otimes|20\rangle_{\mathrm{A}}}\\
&+\sqrt{(n_k+1)(n_f+2)}f^{(2)*}_{|n_k(n_f+1)\rangle_{\mathrm{CRW}}\otimes|10\rangle_{\mathrm{A}}}f^{(3)}_{|(n_k+1)(n_f+2)\rangle_{\mathrm{CRW}}\otimes|10\rangle_{\mathrm{A}}}\\
&+\sqrt{(n_k+1)(n_f-1)}f^{(2)*}_{|n_k(n_f-2)\rangle_{\mathrm{CRW}}\otimes|02\rangle_{\mathrm{A}}}f^{(3)}_{|(n_k+1)(n_f-1)\rangle_{\mathrm{CRW}}\otimes|02\rangle_{\mathrm{A}}}\\
&+\sqrt{(n_k+2)(n_f+1)}f^{(2)*}_{|(n_k+1)n_f\rangle_{\mathrm{CRW}}\otimes|01\rangle_{\mathrm{A}}}f^{(3)}_{|(n_k+2)(n_f+1)\rangle_{\mathrm{CRW}}\otimes|01\rangle_{\mathrm{A}}}\\
&+\sqrt{(n_k+3)(n_f+3)}f^{(2)*}_{|(n_k+2)(n_f+2)\rangle_{\mathrm{CRW}}\otimes|00\rangle_{\mathrm{A}}}f^{(3)}_{|(n_k+3)(n_f+3)\rangle_{\mathrm{CRW}}\otimes|00\rangle_{\mathrm{A}}},
\end{aligned}
$$

$$
\begin{aligned}
\langle a_k\sigma_2\rangle &= \langle\sigma_2 a_k\rangle\\
&= \sqrt{n_k}f^{(1,3)*}_{|(n_k-1)(n_f-1)\rangle_{\mathrm{CRW}}\otimes|00\rangle_{\mathrm{A}}}f^{(1,3)}_{|n_k(n_f-1)\rangle_{\mathrm{CRW}}\otimes|01\rangle_{\mathrm{A}}}+\sqrt{n_k}f^{(1,3)*}_{|(n_k-1)n_f\rangle_{\mathrm{CRW}}\otimes|10\rangle_{\mathrm{A}}}f^{(3)}_{|n_kn_f\rangle_{\mathrm{CRW}}\otimes|11\rangle_{\mathrm{A}}}\\
&\quad+\sqrt{2n_k}f^{(2)*}_{|(n_k-1)(n_f-2)\rangle_{\mathrm{CRW}}\otimes|01\rangle_{\mathrm{A}}}f^{(2)}_{|n_k(n_f-2)\rangle_{\mathrm{CRW}}\otimes|02\rangle_{\mathrm{A}}}+\sqrt{3n_k}f^{(3)*}_{|(n_k-1)(n_f-3)\rangle_{\mathrm{CRW}}\otimes|02\rangle_{\mathrm{A}}}f^{(3)}_{|n_k(n_f-3)\rangle_{\mathrm{CRW}}\otimes|03\rangle_{\mathrm{A}}}\\
&\quad+\sqrt{n_k+1}f^{(0,2)*}_{|n_kn_f\rangle_{\mathrm{CRW}}\otimes|00\rangle_{\mathrm{A}}}f^{(2)}_{|(n_k+1)n_f\rangle_{\mathrm{CRW}}\otimes|01\rangle_{\mathrm{A}}}+\sqrt{2(n_k+1)}f^{(1,3)*}_{|n_k(n_f-1)\rangle_{\mathrm{CRW}}\otimes|01\rangle_{\mathrm{A}}}f^{(3)}_{|(n_k+1)(n_f-1)\rangle_{\mathrm{CRW}}\otimes|02\rangle_{\mathrm{A}}}\\
&\quad+\sqrt{n_k+2}f^{(1,3)*}_{|(n_k+1)(n_f+1)\rangle_{\mathrm{CRW}}\otimes|00\rangle_{\mathrm{A}}}f^{(3)}_{|(n_k+2)(n_f+1)\rangle_{\mathrm{CRW}}\otimes|01\rangle_{\mathrm{A}}}+\sqrt{n_k-1}f^{(2)*}_{|(n_k-2)(n_f-1)\rangle_{\mathrm{CRW}}\otimes|10\rangle_{\mathrm{A}}}f^{(2)}_{|(n_k-1)(n_f-1)\rangle_{\mathrm{CRW}}\otimes|11\rangle_{\mathrm{A}}}\\
&\quad+\sqrt{n_k-1}f^{(2)*}_{|(n_k-2)(n_f-2)\rangle_{\mathrm{CRW}}\otimes|00\rangle_{\mathrm{A}}}f^{(2)}_{|(n_k-1)(n_f-2)\rangle_{\mathrm{CRW}}\otimes|01\rangle_{\mathrm{A}}}+\sqrt{2(n_k-1)}f^{(3)*}_{|(n_k-2)(n_f-2)\rangle_{\mathrm{CRW}}\otimes|11\rangle_{\mathrm{A}}}f^{(3)}_{|(n_k-1)(n_f-2)\rangle_{\mathrm{CRW}}\otimes|12\rangle_{\mathrm{A}}}\\
&\quad+\sqrt{2(n_k-1)}f^{(3)*}_{|(n_k-2)(n_f-3)\rangle_{\mathrm{CRW}}\otimes|01\rangle_{\mathrm{A}}}f^{(3)}_{|(n_k-1)(n_f-3)\rangle_{\mathrm{CRW}}\otimes|02\rangle_{\mathrm{A}}}+\sqrt{n_k-2}f^{(3)*}_{|(n_k-3)(n_f-1)\rangle_{\mathrm{CRW}}\otimes|20\rangle_{\mathrm{A}}}f^{(3)}_{|(n_k-2)(n_f-1)\rangle_{\mathrm{CRW}}\otimes|21\rangle_{\mathrm{A}}}\\
&\quad+\sqrt{n_k-2}f^{(3)*}_{|(n_k-3)(n_f-2)\rangle_{\mathrm{CRW}}\otimes|10\rangle_{\mathrm{A}}}f^{(3)}_{|(n_k-2)(n_f-2)\rangle_{\mathrm{CRW}}\otimes|11\rangle_{\mathrm{A}}}+\sqrt{n_k-2}f^{(3)*}_{|(n_k-3)(n_f-3)\rangle_{\mathrm{CRW}}\otimes|00\rangle_{\mathrm{A}}}f^{(3)}_{|(n_k-2)(n_f-3)\rangle_{\mathrm{CRW}}\otimes|01\rangle_{\mathrm{A}}},\\
\langle a_f\sigma_1\rangle &= \langle\sigma_1 a_f\rangle\\
&= \sqrt{n_f}f^{(1,3)*}_{|(n_k-1)(n_f-1)\rangle_{\mathrm{CRW}}\otimes|00\rangle_{\mathrm{A}}}f^{(1,3)}_{|(n_k-1)n_f\rangle_{\mathrm{CRW}}\otimes|10\rangle_{\mathrm{A}}}+\sqrt{n_f}f^{(1,3)*}_{|n_k(n_f-1)\rangle_{\mathrm{CRW}}\otimes|01\rangle_{\mathrm{A}}}f^{(3)}_{|n_kn_f\rangle_{\mathrm{CRW}}\otimes|11\rangle_{\mathrm{A}}}\\
&\quad+\sqrt{2n_f}f^{(2)*}_{|(n_k-2)(n_f-1)\rangle_{\mathrm{CRW}}\otimes|10\rangle_{\mathrm{A}}}f^{(2)}_{|(n_k-2)n_f\rangle_{\mathrm{CRW}}\otimes|20\rangle_{\mathrm{A}}}+\sqrt{3n_f}f^{(3)*}_{|(n_k-3)(n_f-1)\rangle_{\mathrm{CRW}}\otimes|20\rangle_{\mathrm{A}}}f^{(3)}_{|(n_k-3)n_f\rangle_{\mathrm{CRW}}\otimes|30\rangle_{\mathrm{A}}}\\
&\quad+\sqrt{n_f+1}f^{(0,2)*}_{|n_kn_f\rangle_{\mathrm{CRW}}\otimes|00\rangle_{\mathrm{A}}}f^{(2)}_{|n_k(n_f+1)\rangle_{\mathrm{CRW}}\otimes|10\rangle_{\mathrm{A}}}+\sqrt{2(n_f+1)}f^{(1,3)*}_{|(n_k-1)n_f\rangle_{\mathrm{CRW}}\otimes|10\rangle_{\mathrm{A}}}f^{(3)}_{|(n_k-1)(n_f+1)\rangle_{\mathrm{CRW}}\otimes|20\rangle_{\mathrm{A}}}\\
&\quad+\sqrt{n_f+2}f^{(1,3)*}_{|(n_k+1)(n_f+1)\rangle_{\mathrm{CRW}}\otimes|00\rangle_{\mathrm{A}}}f^{(3)}_{|(n_k+1)(n_f+2)\rangle_{\mathrm{CRW}}\otimes|10\rangle_{\mathrm{A}}}+\sqrt{n_f-1}f^{(2)*}_{|(n_k-1)(n_f-2)\rangle_{\mathrm{CRW}}\otimes|01\rangle_{\mathrm{A}}}f^{(2)}_{|(n_k-1)(n_f-1)\rangle_{\mathrm{CRW}}\otimes|11\rangle_{\mathrm{A}}}\\
&\quad+\sqrt{n_f-1}f^{(2)*}_{|(n_k-2)(n_f-2)\rangle_{\mathrm{CRW}}\otimes|00\rangle_{\mathrm{A}}}f^{(2)}_{|(n_k-2)(n_f-1)\rangle_{\mathrm{CRW}}\otimes|10\rangle_{\mathrm{A}}}+\sqrt{2(n_f-1)}f^{(3)*}_{|(n_k-2)(n_f-2)\rangle_{\mathrm{CRW}}\otimes|11\rangle_{\mathrm{A}}}f^{(3)}_{|(n_k-2)(n_f-1)\rangle_{\mathrm{CRW}}\otimes|21\rangle_{\mathrm{A}}}\\
&\quad+\sqrt{2(n_f-1)}f^{(3)*}_{|(n_k-3)(n_f-2)\rangle_{\mathrm{CRW}}\otimes|10\rangle_{\mathrm{A}}}f^{(3)}_{|(n_k-3)(n_f-1)\rangle_{\mathrm{CRW}}\otimes|20\rangle_{\mathrm{A}}}+\sqrt{n_f-2}f^{(3)*}_{|(n_k-1)(n_f-3)\rangle_{\mathrm{CRW}}\otimes|02\rangle_{\mathrm{A}}}f^{(3)}_{|(n_k-1)(n_f-2)\rangle_{\mathrm{CRW}}\otimes|12\rangle_{\mathrm{A}}}\\
&\quad+\sqrt{n_f-2}f^{(3)*}_{|(n_k-2)(n_f-3)\rangle_{\mathrm{CRW}}\otimes|01\rangle_{\mathrm{A}}}f^{(3)}_{|(n_k-2)(n_f-2)\rangle_{\mathrm{CRW}}\otimes|11\rangle_{\mathrm{A}}}+\sqrt{n_f-2}f^{(3)*}_{|(n_k-3)(n_f-3)\rangle_{\mathrm{CRW}}\otimes|00\rangle_{\mathrm{A}}}f^{(3)}_{|(n_k-3)(n_f-2)\rangle_{\mathrm{CRW}}\otimes|10\rangle_{\mathrm{A}}},\\
\langle a_k\sigma_1\rangle &= \langle\sigma_1 a_k\rangle=0,\\
\langle a_f\sigma_2\rangle &= \langle\sigma_2 a_f\rangle=0.
\end{aligned}
$$

The corresponding coefficients f of Section 3 are as follows:

$$
\begin{aligned}
f^{(0,2)}_{|n_kn_f\rangle_{\mathrm{CRW}}\otimes|00\rangle_{\mathrm{A}}} &= 1-\frac{(2n_kn_f+n_k+n_f+1)g_0^2}{8}t^2-\frac{n_kg_1^2}{2N_{\mathrm{c}}}\sum_k\left[2+\mathrm{e}^{\mathrm{i}k(n_1-n_2)}+\mathrm{e}^{\mathrm{i}k(n_2-n_1)}\right]t^2\\
&\quad-\frac{n_fg_2^2}{2N_{\mathrm{c}}}\sum_f\left[2+\mathrm{e}^{\mathrm{i}f(m_1-m_2)}+\mathrm{e}^{\mathrm{i}f(m_2-m_1)}\right]t^2,\\
f^{(1,3)}_{|(n_k-1)n_f\rangle_{\mathrm{CRW}}\otimes|10\rangle_{\mathrm{A}}} &= -\frac{\mathrm{i}\sqrt{n_k}g_1}{\sqrt{N_{\mathrm{c}}}}\sum_k\left(\mathrm{e}^{\mathrm{i}kn_1}+\mathrm{e}^{\mathrm{i}kn_2}\right)t+\frac{\mathrm{i}\left(6n_kn_f+3n_k+2\right)\sqrt{n_k}g_1g_0^2}{24\sqrt{Nc}}\sum_k\left(\mathrm{e}^{\mathrm{i}kn_1}+\mathrm{e}^{\mathrm{i}kn_2}\right)t^3\\
&\quad+\frac{\mathrm{i}\left(3n_k-2\right)\sqrt{n_k}g_1^3}{6N_{\mathrm{c}}\sqrt{N_{\mathrm{c}}}}\sum_k\left[3\mathrm{e}^{\mathrm{i}kn_1}+3\mathrm{e}^{\mathrm{i}kn_2}+\mathrm{e}^{\mathrm{i}k(2n_1-n_2)}+\mathrm{e}^{\mathrm{i}k(2n_2-n_1)}\right]t^3\\
&\quad+\frac{\mathrm{i}n_f\sqrt{n_k}g_1g_2^2}{2N_{\mathrm{c}}\sqrt{N_{\mathrm{c}}}}\sum_k\left(\mathrm{e}^{\mathrm{i}kn_1}+\mathrm{e}^{\mathrm{i}kn_2}\right)\sum_f\left[2+\mathrm{e}^{\mathrm{i}f(m_1-m_2)}+\mathrm{e}^{\mathrm{i}f(m_2-m_1)}\right]t^3,\\
f^{(1,3)}_{|n_k(n_f-1)\rangle_{\mathrm{CRW}}\otimes|01\rangle_{\mathrm{A}}} &= -\frac{\mathrm{i}\sqrt{n_f}g_2}{\sqrt{N_{\mathrm{c}}}}\sum_f\left(\mathrm{e}^{\mathrm{i}fm_1}+\mathrm{e}^{\mathrm{i}fm_2}\right)t+\frac{\mathrm{i}\left(6n_kn_f+3n_f+2\right)\sqrt{n_f}g_2g_0^2}{24\sqrt{Nc}}\sum_f\left(\mathrm{e}^{\mathrm{i}km_1}+\mathrm{e}^{\mathrm{i}km_2}\right)t^3\\
&\quad+\frac{\mathrm{i}\left(3n_f-2\right)\sqrt{n_f}g_2^3}{6N_{\mathrm{c}}\sqrt{N_{\mathrm{c}}}}\sum_f\left[3\mathrm{e}^{\mathrm{i}fm_1}+3\mathrm{e}^{\mathrm{i}fm_2}+\mathrm{e}^{\mathrm{i}f(2m_1-m_2)}+\mathrm{e}^{\mathrm{i}f(2m_2-m_1)}\right]t^3
\end{aligned}
$$

$$
\begin{aligned}
&+\frac{\mathrm{i}n_k\sqrt{n_f}g_2g_1^2}{2N_\mathrm{c}\sqrt{N_\mathrm{c}}}\sum_f\left(\mathrm{e}^{\mathrm{i}fm_1}+\mathrm{e}^{\mathrm{i}fm_2}\right)\sum_k\left[2+\mathrm{e}^{\mathrm{i}k(n_1-n_2)}+\mathrm{e}^{\mathrm{i}k(n_2-n_1)}\right]t^3,\\
f^{(1,3)}_{|(n_k+1)(n_f+1)\rangle_{\mathrm{CRW}}\otimes|00\rangle_{\mathrm{A}}} &= -\frac{\mathrm{i}g_0\sqrt{(n_k+1)\left(n_f+1\right)}}{2}t+\frac{\mathrm{i}\left(3n_kn_f+3n_k+3n_f+5\right)\sqrt{(n_k+1)\left(n_f+1\right)}g_0^3}{48}t^3\\
&+\frac{\mathrm{i}\left(3n_k+1\right)\sqrt{(n_k+1)\left(n_f+1\right)}g_1^2g_0}{12N_\mathrm{c}}\sum_k\left[2+\mathrm{e}^{\mathrm{i}k(n_1-n_2)}+\mathrm{e}^{\mathrm{i}k(n_2-n_1)}\right]t^3\\
&+\frac{\mathrm{i}\left(3n_f+1\right)\sqrt{(n_k+1)\left(n_f+1\right)}g_2^2g_0}{12N_\mathrm{c}}\sum_f\left[2+\mathrm{e}^{\mathrm{i}f(m_1-m_2)}+\mathrm{e}^{\mathrm{i}f(m_2-m_1)}\right]t^3,\\
f^{(1,3)}_{|(n_k-1)(n_f-1)\rangle_{\mathrm{CRW}}\otimes|00\rangle_{\mathrm{A}}} &= -\frac{\mathrm{i}g_0\sqrt{n_kn_f}}{2}t+\frac{\mathrm{i}\left(3n_kn_f+2\right)\sqrt{n_kn_f}g_0^3}{48}t^3+\frac{\mathrm{i}\left(3n_k-2\right)\sqrt{n_kn_f}g_1^2g_0}{12N_\mathrm{c}}\sum_k\left[2+\mathrm{e}^{\mathrm{i}k(n_1-n_2)}+\mathrm{e}^{\mathrm{i}k(n_2-n_1)}\right]t^3\\
&+\frac{\mathrm{i}\left(3n_f-2\right)\sqrt{n_kn_f}g_2^2g_0}{12N_\mathrm{c}}\sum_f\left[2+\mathrm{e}^{\mathrm{i}f(m_1-m_2)}+\mathrm{e}^{\mathrm{i}f(m_2-m_1)}\right]t^3,\\
f^{(2)}_{|(n_k-2)n_f\rangle_{\mathrm{CRW}}\otimes|20\rangle_{\mathrm{A}}} &= -\frac{\sqrt{2n_k\left(n_k-1\right)}g_1^2}{2N_\mathrm{c}}\sum_k\left[\mathrm{e}^{2\mathrm{i}kn_1}+\mathrm{e}^{2\mathrm{i}kn_2}+2\mathrm{e}^{\mathrm{i}k(n_1+n_2)}\right]t^2,\\
f^{(2)}_{|(n_k-1)(n_f-1)\rangle_{\mathrm{CRW}}\otimes|11\rangle_{\mathrm{A}}} &= -\frac{\sqrt{n_kn_f}g_1g_2}{N_\mathrm{c}}\sum_k\left(\mathrm{e}^{\mathrm{i}kn_1}+\mathrm{e}^{\mathrm{i}kn_2}\right)\sum_f\left(\mathrm{e}^{\mathrm{i}fm_1}+\mathrm{e}^{\mathrm{i}fm_2}\right)t^2,\\
f^{(2)}_{|n_k(n_f+1)\rangle_{\mathrm{CRW}}\otimes|10\rangle_{\mathrm{A}}} &= -\frac{\left(2n_k+1\right)\sqrt{n_f+1}g_1g_0}{4\sqrt{N_\mathrm{c}}}\sum_k\left(\mathrm{e}^{\mathrm{i}kn_1}+\mathrm{e}^{\mathrm{i}kn_2}\right)t^2,\\
f^{(2)}_{|(n_k-2)(n_f-1)\rangle_{\mathrm{CRW}}\otimes|10\rangle_{\mathrm{A}}} &= -\frac{\sqrt{n_kn_f\left(n_k-1\right)}g_1g_0}{2\sqrt{N_\mathrm{c}}}\sum_k\left(\mathrm{e}^{\mathrm{i}kn_1}+\mathrm{e}^{\mathrm{i}kn_2}\right)t^2,\\
f^{(2)}_{|n_k(n_f-2)\rangle_{\mathrm{CRW}}\otimes|02\rangle_{\mathrm{A}}} &= -\frac{\sqrt{2n_f\left(n_f-1\right)}g_2^2}{2N_\mathrm{c}}\sum_f\left[\mathrm{e}^{2\mathrm{i}fm_1}+\mathrm{e}^{2\mathrm{i}fm_2}+2\mathrm{e}^{\mathrm{i}f(m_1+m_2)}\right]t^2,\\
f^{(2)}_{|(n_k+1)n_f\rangle_{\mathrm{CRW}}\otimes|01\rangle_{\mathrm{A}}} &= -\frac{\left(2n_f+1\right)\sqrt{n_k+1}g_2g_0}{4\sqrt{N_\mathrm{c}}}\sum_f\left(\mathrm{e}^{\mathrm{i}fm_1}+\mathrm{e}^{\mathrm{i}fm_2}\right)t^2,\\
f^{(2)}_{|(n_k-1)(n_f-2)\rangle_{\mathrm{CRW}}\otimes|01\rangle_{\mathrm{A}}} &= -\frac{\sqrt{n_kn_f\left(n_f-1\right)}g_2g_0}{2\sqrt{N_\mathrm{c}}}\sum_f\left(\mathrm{e}^{\mathrm{i}fm_1}+\mathrm{e}^{\mathrm{i}fm_2}\right)t^2,\\
f^{(2)}_{|(n_k+2)(n_f+2)\rangle_{\mathrm{CRW}}\otimes|00\rangle_{\mathrm{A}}} &= -\frac{\sqrt{(n_k+1)\left(n_k+2\right)\left(n_f+1\right)\left(n_f+2\right)}g_0^2}{8}t^2,\\
f^{(2)}_{|(n_k-2)(n_f-2)\rangle_{\mathrm{CRW}}\otimes|00\rangle_{\mathrm{A}}} &= -\frac{\sqrt{n_kn_f\left(n_k-1\right)\left(n_f-1\right)}g_0^2}{8}t^2,\\
f^{(3)}_{|(n_k-3)n_f\rangle_{\mathrm{CRW}}\otimes|30\rangle_{\mathrm{A}}} &= \frac{\mathrm{i}\sqrt{6n_k\left(n_k-1\right)\left(n_k-2\right)}g_1^3}{6N_\mathrm{c}\sqrt{N_\mathrm{c}}}\sum_k\left[\mathrm{e}^{3\mathrm{i}kn_1}+\mathrm{e}^{3\mathrm{i}kn_2}\right]t^3+\frac{\mathrm{i}\sqrt{6n_k\left(n_k-1\right)\left(n_k-2\right)}g_1^3}{6N_\mathrm{c}\sqrt{N_\mathrm{c}}}\sum_k\left[3\mathrm{e}^{\mathrm{i}k(2n_1+n_2)}+3\mathrm{e}^{\mathrm{i}k(2n_2+n_1)}\right]t^3,\\
f^{(3)}_{|(n_k-2)(n_f-1)\rangle_{\mathrm{CRW}}\otimes|21\rangle_{\mathrm{A}}} &= \frac{\mathrm{i}\sqrt{2n_kn_f\left(n_k-1\right)}g_1^2g_2}{2N_\mathrm{c}\sqrt{N_\mathrm{c}}}\sum_k\left[\mathrm{e}^{2\mathrm{i}kn_1}+\mathrm{e}^{2\mathrm{i}kn_2}+2\mathrm{e}^{\mathrm{i}k(n_1+n_2)}\right]\sum_f\left(\mathrm{e}^{\mathrm{i}fm_1}+\mathrm{e}^{\mathrm{i}fm_2}\right)t^3,\\
f^{(3)}_{|(n_k-1)(n_f+1)\rangle_{\mathrm{CRW}}\otimes|20\rangle_{\mathrm{A}}} &= \frac{in_k\sqrt{2n_k\left(n_f+1\right)}g_1^2g_0}{4N_\mathrm{c}}\sum_k\left[\mathrm{e}^{2\mathrm{i}kn_1}+\mathrm{e}^{2\mathrm{i}kn_2}+2\mathrm{e}^{\mathrm{i}k(n_1+n_2)}\right]t^3,\\
f^{(3)}_{|(n_k-3)(n_f-1)\rangle_{\mathrm{CRW}}\otimes|20\rangle_{\mathrm{A}}} &= \frac{\mathrm{i}\sqrt{2n_kn_f\left(n_k-1\right)\left(n_k-2\right)}g_1^2g_0}{4N_\mathrm{c}}\sum_k\left[\mathrm{e}^{2\mathrm{i}kn_1}+\mathrm{e}^{2\mathrm{i}kn_2}+2\mathrm{e}^{\mathrm{i}k(n_1+n_2)}\right]t^3,\\
f^{(3)}_{|(n_k-1)(n_f-2)\rangle_{\mathrm{CRW}}\otimes|12\rangle_{\mathrm{A}}} &= \frac{\mathrm{i}\sqrt{2n_kn_f\left(n_f-1\right)}g_1g_2^2}{2N_\mathrm{c}\sqrt{N_\mathrm{c}}}\sum_f\left[\mathrm{e}^{2\mathrm{i}fm_1}+\mathrm{e}^{2\mathrm{i}fm_2}+2\mathrm{e}^{\mathrm{i}f(m_1+m_2)}\right]\sum_k\left(\mathrm{e}^{\mathrm{i}kn_1}+\mathrm{e}^{\mathrm{i}kn_2}\right)t^3,\\
f^{(3)}_{|n_kn_f\rangle_{\mathrm{CRW}}\otimes|11\rangle_{\mathrm{A}}} &= \frac{\mathrm{i}\left(6n_kn_f+3n_k+3n_f+2\right)g_1g_2g_0}{12N_\mathrm{c}}\sum_k\left(\mathrm{e}^{\mathrm{i}kn_1}+\mathrm{e}^{\mathrm{i}kn_2}\right)\sum_f\left(\mathrm{e}^{\mathrm{i}fm_1}+\mathrm{e}^{\mathrm{i}fm_2}\right)t^3,\\
f^{(3)}_{|(n_k-2)(n_f-2)\rangle_{\mathrm{CRW}}\otimes|11\rangle_{\mathrm{A}}} &= \frac{\mathrm{i}\sqrt{n_kn_f\left(n_k-1\right)\left(n_f-1\right)}g_1g_2g_0}{2N_\mathrm{c}}\sum_k\left(\mathrm{e}^{\mathrm{i}kn_1}+\mathrm{e}^{\mathrm{i}kn_2}\right)\sum_f\left(\mathrm{e}^{\mathrm{i}fm_1}+\mathrm{e}^{\mathrm{i}fm_2}\right)t^3,
\end{aligned}
$$

$$f^{(3)}_{|(n_k+1)(n_f+2)\rangle_{\mathrm{CRW}}\otimes|10\rangle_{\mathrm{A}}} = \frac{\mathrm{i}\,(n_k+1)\sqrt{(n_k+1)\,(n_f+1)\,(n_f+2)}g_1g_0^2}{8\sqrt{N_\mathrm{c}}}\sum_k\left(\mathrm{e}^{\mathrm{i}kn_1}+\mathrm{e}^{\mathrm{i}kn_2}\right)t^3,$$

$$f^{(3)}_{|(n_k-3)(n_f-2)\rangle_{\mathrm{CRW}}\otimes|10\rangle_{\mathrm{A}}} = \frac{\mathrm{i}\sqrt{n_kn_f\,(n_k-1)\,(n_f-1)\,(n_k-2)}g_1g_0^2}{8\sqrt{N_\mathrm{c}}}\sum_k\left(\mathrm{e}^{\mathrm{i}kn_1}+\mathrm{e}^{\mathrm{i}kn_2}\right)t^3,$$

$$\begin{aligned} f^{(3)}_{|n_k(n_f-3)\rangle_{\mathrm{CRW}}\otimes|03\rangle_{\mathrm{A}}} &= \frac{\mathrm{i}\sqrt{6n_f\,(n_f-1)\,(n_f-2)}g_2^3}{6N_\mathrm{c}\sqrt{N_\mathrm{c}}}\sum_f\left[\mathrm{e}^{3\mathrm{i}fm_1}+\mathrm{e}^{3\mathrm{i}fm_2}\right]t^3 \\ &+\frac{\mathrm{i}\sqrt{6n_f\,(n_f-1)\,(n_f-2)}g_2^3}{6N_\mathrm{c}\sqrt{N_\mathrm{c}}}\sum_f\left[3\mathrm{e}^{\mathrm{i}f(2m_1+m_2)}+3\mathrm{e}^{\mathrm{i}f(2m_2+m_1)}\right]t^3, \end{aligned}$$

$$f^{(3)}_{|(n_k+1)(n_f-1)\rangle_{\mathrm{CRW}}\otimes|02\rangle_{\mathrm{A}}} = \frac{in_f\sqrt{2n_f\,(n_k+1)}g_2^2g_0}{4N_\mathrm{c}}\sum_f\left[\mathrm{e}^{2\mathrm{i}fm_1}+\mathrm{e}^{2\mathrm{i}fm_2}+2\mathrm{e}^{\mathrm{i}f(m_1+m_2)}\right]t^3,$$

$$f^{(3)}_{|(n_k-1)(n_f-3)\rangle_{\mathrm{CRW}}\otimes|02\rangle_{\mathrm{A}}} = \frac{\mathrm{i}\sqrt{2n_kn_f\,(n_f-1)\,(n_f-2)}g_2^2g_0}{4N_\mathrm{c}}\sum_f\left[\mathrm{e}^{2\mathrm{i}fm_1}+\mathrm{e}^{2\mathrm{i}fm_2}+2\mathrm{e}^{\mathrm{i}f(m_1+m_2)}\right]t^3,$$

$$f^{(3)}_{|(n_k+2)(n_f+1)\rangle_{\mathrm{CRW}}\otimes|01\rangle_{\mathrm{A}}} = \frac{\mathrm{i}\,(n_f+1)\sqrt{(n_k+1)\,(n_f+1)\,(n_k+2)}g_2g_0^2}{8\sqrt{N_\mathrm{c}}}\sum_f\left(\mathrm{e}^{\mathrm{i}fm_1}+\mathrm{e}^{\mathrm{i}fm_2}\right)t^3,$$

$$f^{(3)}_{|(n_k-2)(n_f-3)\rangle_{\mathrm{CRW}}\otimes|01\rangle_{\mathrm{A}}} = \frac{\mathrm{i}\sqrt{n_kn_f\,(n_k-1)\,(n_f-1)\,(n_f-2)}g_2g_0^2}{8\sqrt{N_\mathrm{c}}}\sum_f\left(\mathrm{e}^{\mathrm{i}fm_1}+\mathrm{e}^{\mathrm{i}fm_2}\right)t^3,$$

$$f^{(3)}_{|(n_k+3)(n_f+3)\rangle_{\mathrm{CRW}}\otimes|00\rangle_{\mathrm{A}}} = \frac{\mathrm{i}\sqrt{(n_k+1)\,(n_k+2)\,(n_k+3)\,(n_f+1)\,(n_f+2)\,(n_f+3)}g_0^3}{48}t^3,$$

$$f^{(3)}_{|(n_k-3)(n_f-3)\rangle_{\mathrm{CRW}}\otimes|00\rangle_{\mathrm{A}}} = \frac{\mathrm{i}\sqrt{n_kn_f\,(n_k-1)\,(n_k-2)\,(n_f-1)\,(n_f-2)}g_0^3}{48}t^3,$$

where $k=2\pi n/N_\mathrm{c}$, with $n=-N_\mathrm{c}/2,-N_\mathrm{c}/2+1,\ldots,N_\mathrm{c}/2-1$, and $f=2\pi m/N_\mathrm{c}$, with $m=-N_\mathrm{c}/2,-N_\mathrm{c}/2+1,\ldots,N_\mathrm{c}/2-1$.

Acknowledgement

Project supported by the Education Department of Jilin Province, China (Grant No. JJKH20231291KJ).

References

[1] Moore G T 1970 *J. Math. Phys.* **11** 2679
[2] Fulling S A and Davies P C W 1976 *Proc. R. Soc. Lond.* **348** 393
[3] Dodonov V V 2010 *Phys. Scr.* **82** 038105
[4] Nation P, Johansson J, Blencowe M and Nori F 2012 *Rev. Mod. Phys.* **84** 1
[5] Yablonovitch E 1989 *Phys. Rev. Lett.* **62** 1742
[6] Uhlmann M, Plunien G, Schützhold R and Soff G 2004 *Phys. Rev. Lett.* **93** 193601
[7] Wilson C M, Johansson G, Pourkabirian A, Simoen M, Johansson J R, Duty T, Nori F and Delsing P 2011 *Nature* **479** 376
[8] Lähteenmäki P, Paraoanu G S, Hassel J and Hakonen P J 2013 *Proc. Natl. Acad. Sci. USA* **110** 4234
[9] Dodonov V V, Klimov A B and Man'ko V I 1990 *Phys. Lett. A* **149** 225
[10] Dodonov V V and Andreata M A 1999 *J. Phys. A* **32** 6711
[11] Johansson J R, Johansson G, Wilson C M and Nori F 2010 *Phys. Rev. A* **82** 052509
[12] Andreata M A and Dodonov V V 2005 *J. Opt. B: Quantum Semiclass. Opt.* **7** S11
[13] Felicetti S, Sanz M, Lamata L, Romero G, Johansson G, Delsing P and Solano E 2014 *Phys. Rev. Lett.* **113** 093602
[14] Busch X, Parentani R and Robertson S 2014 *Phys. Rev. A* **89** 063606
[15] Samos Sáenz de Buruaga N and Sabín C 2017 *Phys. Rev. A* **95** 022307
[16] Agustí A, Solano E and Sabín C 2019 *Phys. Rev. A* **99** 052328
[17] Ollivier H and Zurek W H 2001 *Phys. Rev. Lett.* **88** 017901
[18] Zurek W H 2003 *Phys. Rev. A* **67** 012320
[19] Sabín C, Fuentes I and Johansson G 2015 *Phys. Rev. A* **92** 012314
[20] Wiseman H M, Jones S J and Doherty A C 2007 *Phys. Rev. Lett.* **98** 140402
[21] Cavalcanti E G, Jones S J, Wiseman H M and Reid M D 2009 *Phys. Rev. A* **80** 032112
[22] Bowles J, Vértesi T, Quintino M T and Brunner N 2014 *Phys. Rev. Lett.* **112** 200402
[23] Li C M, Chen Y N and Lambert N, Chiu C Y and Nori F 2015 *Phys. Rev. A* **92** 062310
[24] Xiao Y, Ye X J, Sun K, Xu J S, Li C F and Guo G C 2017 *Phys. Rev. Lett.* **118** 140404
[25] Wang M, Xiang Y, Kang H, Han D, Liu Y, He Q, Gong Q, Su X and Peng K 2020 *Phys. Rev. Lett.* **125** 260506
[26] Li J, Zhou Y and Wang Q 2022 *Chin. Phys. Lett.* **39** 110301
[27] Chen Y Y, Guo F Z, Wei S H and Wen Q Y 2023 *Chin. Phys. B* **32** 040309
[28] Hu M J, Hu X M and Zhang Y S 2024 *Chin. Phys. Lett.* **41** 050302
[29] Schrödinger E 1935 *Proc. Cambridge Philos. Soc.* **31** 555
[30] Einstein A, Podolsky B and Rosen N 1935 *Phys. Rev.* **47** 777
[31] Bell J S 1964 *Physics Physique Fizika* **1** 195
[32] Branciard C, Cavalcanti E G, Walborn S P, Scarani V and Wiseman H M 2012 *Phys. Rev. A* **85** 010301
[33] Gallego R and Aolita L 2015 *Phys. Rev. X* **5** 041008
[34] Walk N, Hosseini S, Geng J, Thearle O, Haw J Y, Armstrong S, Assad S M, Janousek J, Ralph T C, Symul T, Wiseman H M and Lam P K 2016 *Optica* **3** 634
[35] Reid M D 2013 *Phys. Rev. A* **88** 062338
[36] He Q, Rosales-Zárate L, Adesso G and Reid M D 2015 *Phys. Rev. Lett.* **115** 180502
[37] Daniel C, Paul S and Ivan S 2017 *Phys. Rev. Lett.* **119** 110501
[38] Piani M and Watrous J 2015 *Phys. Rev. Lett.* **114** 060404
[39] Gisin N and Thew R 2007 *Nat. Photon.* **1** 3
[40] He Q Y and Reid M D 2013 *Phys. Rev. Lett.* **111** 250403
[41] Deng X, Xiang Y, Tian C, Adesso G, He Q, Gong Q, Su X, Xie C and Peng K 2017 *Phys. Rev. Lett.* **118** 230501
[42] Xiang Y, Liu Y, Cai Y, Li F, Zhang Y and He Q 2020 *Phys. Rev. A* **101** 053834

[43] Cai Y, Xiang Y, Liu Y, He Q Y and Treps N 2020 *Phys. Rev. Res.* **2** 032046
[44] Zhou L, Dong H, Liu Y X and Sun C P and Nori F 2008 *Phys. Rev. A* **78** 063827
[45] Hoi I C, Wilson C M, Johansson G, Palomaki T, Peropadre B and Delsing P 2011 *Phys. Rev. Lett.* **107** 073601
[46] Cheng M T, Ma X S, Ding M T, Luo Y Q and Zhao G X 2012 *Phys. Rev. A* **85** 053840
[47] Wang Z J and Qi J X 2019 *Optik* **186**
[48] Gustafsson M V, Aref T, Kockum A F, Ekström M K, Johansson G and Delsing P 2014 *Science* **346** 207
[49] Kockum A F, Delsing P and Johansson G 2014 *Phys. Rev. A* **90** 013837
[50] Manenti R, Kockum A F, Patterson A, Behrle T, Rahamim J, Tancredi G, Nori F and Leek P J 2017 *Nat. Commun.* **8** 975
[51] Guo L, Grimsmo A, Kockum A F, Pletyukhov M and Johansson G 2017 *Phys. Rev. A* **95** 053821
[52] Andersson G, Suri B, Guo L, Aref T and Delsing P 2019 *Nat. Phys.* **15** 1123
[53] Wen P Y, Kockum A F, Ian H, Chen J C, Nori F and Hoi I C 2018 *Phys. Rev. Lett.* **120** 063603
[54] Kannan B, Ruckriegel M J, Campbell D L, Kockum A F, Braumüller J, Kim D K, Kjaergaard M, Krantz P, Melville A, Niedzielski B M, Vepsäläinen A, Winik R, Yoder J L, Nori F, Orlando T P, Gustavsson S and Oliver W D 2020 *Nature* **583** 7818
[55] Vadiraj A M, Ask Andreas, McConkey T G, Nsanzineza I, Sandbo Chang C W, Kockum Anton Frisk and Wilson C M 2021 *Phys. Rev. A* **103** 023710
[56] González-Tudela A, Muñoz C S and Cirac J I 2019 *Phys. Rev. Lett.* **122** 203603
[57] Yin X L, Liu Y H, Huang J F and Liao J Q 2022 *Phys. Rev. A* **106** 013715
[58] Yin X L and Liao J Q 2023 *Phys. Rev. A* **108** 023728
[59] Santos A C and Bachelard R 2023 *Phys. Rev. Lett.* **130** 053601
[60] Guo S, Wang Y, Purdy T and Taylor J 2020 *Phys. Rev. A* **102** 033706
[61] Kockum A F, Johansson G and Nori F 2018 *Phys. Rev. Lett.* **120** 140404
[62] Carollo A, Cilluffo D and Ciccarello F 2020 *Phys. Rev. Res.* **2** 043184
[63] Soro A and Kockum A F 2022 *Phys. Rev. A* **105** 023712
[64] Rossatto D Z, Felicetti S, Eneriz H, Rico E, Sanz M and Solano E 2016 *Phys. Rev. B* **93** 094514
[65] Reid M D 1989 *Phys. Rev. A* **40** 913
[66] Reid M D, Drummond P D, Bowen W P, Cavalcanti E G, Lam P K, Bachor H A, Andersen U L and Leuchs G 2009 *Rev. Mod. Phys.* **81** 1727
[67] Yin X L and Liao J Q 2023 *Phys. Rev. A* **108** 023728
[68] Paternostro M, Son W and Kim M S 2004 *Phys. Rev. Lett.* **92** 197901
[69] Augusiak R, Demianowicz M, Pawłowski M, Tura J and Acín A 2014 *Phys. Rev. A* **90** 052323